



1 **Climate change impacts on floods in West Africa: New insight from**
2 **two large-scale hydrological models**

3

4

5 Serigne Bassirou Diop 1

6 Job Ekolu 2

7 Yves Trambly 3

8 Bastien Dieppois 2

9 Stefania Grimaldi 4

10 Ansoumana Bodian 1

11 Juliette Blanchet 5

12 Ponnambalam Rameshwaran 6

13 Peter Salamon 4

14 Benjamin Sultan 3

15

16 1 Laboratoire Leïdi “Dynamique des Territoires et Développement”, Université Gaston Berger,

17 Saint-Louis, Senegal

18

19 2 Centre for Agroecology, Water and Resilience, Coventry University, Coventry, UK

20

21 3 Espace-Dev, Univ. Montpellier, IRD, Montpellier, France

22

23 4 European Commission, Joint Research Centre (JRC), Ispra, Italy

24

25 5 Univ. Grenoble Alpes, CNRS, IRD, Grenoble INP, IGE, Grenoble, France

26

27 6 UK Centre for Ecology & Hydrology, Wallingford, UK

28

29 *Correspondence to: Serigne Bassirou Diop (09.bachir.diop.10@gmail.com)*

30

31

32

33



34 **Abstract**

35

36 West Africa is projected to face unprecedented shifts in temperature and extreme precipitation
37 patterns as a result of climate change. The devastating impacts of river flooding are already
38 being felt in most West African countries, emphasizing the urgent need for comprehensive
39 insights into the frequency and magnitude of floods to guide the design of hydraulic
40 infrastructure for effective flood risk mitigation and water resource management. Despite its
41 significant socio-economic and environmental impacts, flood hazards remain poorly
42 documented in West Africa due to the data-related challenges. This study aims to fill this
43 knowledge gap by providing a large-scale analysis of flood frequency and magnitudes across
44 West Africa, focusing on how climate change may influence future flood trends. To achieve
45 this, we have used two large-scale hydrological models driven by five bias-corrected CMIP6
46 climate models under two Shared Socioeconomic Pathways (SSPs). The Generalized Extreme
47 Value (GEV) distribution was utilized to analyze trends and detect change points by comparing
48 multiple non-stationary GEV models across historical and future periods for a set of 58
49 catchments. Both hydrological models consistently projected increases in flood frequency and
50 magnitude across West Africa, despite their differences in hydrological processes
51 representation and calibration schemes. Flood magnitude is projected to increase for 94 % of
52 the stations, with some locations experiencing increases exceeding 45 % in magnitude. In
53 addition, the majority of trends are starting from the historical period, under both SSP2-4.5 and
54 SSP5-8.5. The findings from this study provide regional-scale insights into the evolving flood
55 risks across West Africa and highlight the urgent need for climate-resilient strategies to
56 safeguard populations and infrastructure against the increasing threat of flood hazards.

57

58 **Keywords:** Flood frequency analysis, GEV, GMLE, West Africa, climate change, CMIP, SSP



59 **1 Introduction**

60 Anthropogenic changes in atmospheric composition and land use have led to climate change
61 (Houghton et al., 2001; Hansen et al., 2010; Santer et al., 2019; Masson-Delmotte et al., 2021).
62 Climate change, in turn, amplifies the frequency, intensity, and impact of extreme events, such
63 as heatwaves, storms, floods, and droughts at the global scale (IPCC, 2021). West Africa is
64 identified as a hotspot for climate change impacts, as the region is projected to experience
65 unprecedented shifts in both temperature and extreme precipitation patterns (IPCC, 2021). West
66 African populations are therefore becoming increasingly vulnerable for floods and droughts
67 (Tramblay et al., 2020, Rameshwaran et al., 2021). This vulnerability is due to multiple factors such
68 as the region's reliance on rainfed agriculture and the dependence of its rural communities on
69 the natural environment (Krishnamurthy et al., 2012; Totin et al., 2016; Land et al., 2018; Diallo
70 et al., 2020; De Longueville et al., 2020; Matthew et al., 2020). Additionally, the limited economic and
71 institutional resources available to manage and adapt to climate change and natural hazards
72 exacerbate this vulnerability (Roudier et al., 2011; Sultan & Gaetani, 2016; Lalou et al., 2019).

73

74 A potential increase in river flooding risks is one of the most frequently studied impacts of
75 climate change (Arnell & Gosling, 2016), because of the devastating economic and
76 environmental impacts it may trigger (EM-DAT, 2015; CRED, 2022; UNDRR, 2023). Such
77 impacts of climate change are already being felt in many West African countries, which
78 experienced several catastrophic floods in the past few years, raising concerns for water
79 management and livelihoods (World Bank, 2021a). It is therefore becoming crucial to develop
80 efficient adaptation strategies for mitigating the adverse effects of flood hazards on West
81 African communities and economies.

82

83 Efficient water resources management is essential for sustainable development in West Africa
84 in a changing climate (UNEP, 2020). However, water management requires comprehensive
85 insights into the frequency and magnitude of floods to design appropriate hydraulic
86 infrastructure (Feaster et al., 2023), and quantification of watershed runoff to design reservoirs
87 for agricultural, industrial, and municipal water use (Song et al., 2022). In West Africa however,
88 access to hydrometric data remains a challenge, as the number of stations within hydro-
89 monitoring networks has decreased in recent years (Bodian et al., 2020; Tarpanelli et al., 2023).
90 Existing hydrometric databases, available to estimate design flows, only provide short and
91 often old records (Agoungbome et al., 2018; Tramblay et al., 2021). Therefore, updating these



92 hydrological standards is essential to ensure that they accurately represent the current
93 hydroclimatic context of the region (Wasko et al., 2021).

94

95 Global Climate Models (GCMs) outputs from the fifth/sixth Coupled Model Intercomparison
96 Project (CMIP5/6), which contributed to the fifth and sixth Assessment Report (AR5/6) of the
97 Intergovernmental Panel on Climate Change (IPCC), have provided opportunities to simulate
98 future hydrological impacts of climate change worldwide. Indeed, CMIP5/6 models use a range
99 of scenarios that represent different future trajectories to simulate several climate variables,
100 which help researchers assess the potential long-term impacts of near-term decisions on
101 emissions reductions and climate policies (Riahi et al., 2017). To understand future trends in
102 hydrological extremes, climate models are typically used in combination with hydrological
103 modelling experiments. However, the simulations from GCMs cannot be used directly to drive
104 hydrological models as they are associated with systematic biases relative to observational
105 datasets (Sillmann et al., 2013). Therefore, downscaling and bias-correction algorithms are
106 routinely applied to leverage the information from GCM outputs (Ehret et al., 2012).
107 Nevertheless, large uncertainties remain regarding future climate trends in West Africa, due to
108 the sensitivity of different climate models contrasting warming in the North Atlantic and
109 Mediterranean Sea, which are known to influence the West African Monsoon (Bichet et al.,
110 2020; Monerie et al., 2023), and due to contrasting emission scenarios (IPCC, 2021).

111

112 As climate change may intensify the hydrological cycle (Gudmundsson et al., 2012),
113 systematically assessing future flood risks and regional-scale hydrological impacts of future
114 climate change is crucial for developing effective climate adaptation strategies (Huang et al.,
115 2024). The interest in large-scale hydrological models has increased due to the need to
116 sustainably manage large river basins and the pervasive global environmental change (Döll et
117 al., 2008). As global hydrological models can capture the variability of hydrological processes
118 across different geographical and climatic contexts, large-scale hydrological modelling has
119 become a key tool for analysing global and regional water resources, assessing climate impacts,
120 and managing water resources (Kauffeldt et al., 2013; Prudhomme et al., 2024). However,
121 running physically based large-scale hydrological models requires numerous input variables
122 that describe the physiographic characteristics of the watersheds (such as soil moisture, land
123 use/land cover, topography, etc.), along with several meteorological forcings. Thus, this
124 complexity limits the widespread use of these models. Brunner et al. (2021) have argued that
125 the limited information on regional flood trends is partly due to the data-related challenges. In



126 the West African context, several studies have shown the increase in extreme rainfall in
127 observations (Taylor et al., 2017, Trambly et al., 2020, Chagnaud et al., 2022) and future
128 climate scenarios (Dosio et al., 2021, Chagnaud et al., 2023), but very few studies have used
129 GCMs simulations as forcings to drive grid-based large-scale hydrological models to assess
130 the potential impacts of climate change on river flows across West Africa (Rameshwaran et al.,
131 2021; Ekolu et al., 2024, <https://africa-hydrology.ceh.ac.uk/>). The main objective of this study
132 is to address this gap by assessing the impacts of climate change on floods in the West African
133 region from two large-scale hydrological models driven by data from five bias-corrected
134 CMIP6 GCMs under two Shared Socioeconomic Pathways (SSPs; O'Neill et al., 2017). This
135 article is organised as follows: In Section 2, we describe the study area. Section 3 outlines the
136 materials and methods, including the data used in the analysis, the CMIP6 models and
137 hydrological modelling approach, the non-stationary extreme value analysis framework, and
138 the evaluation of climate change impacts on floods at both local and regional scales. In Section
139 4, we present and discuss the findings. Finally, main conclusions and perspectives are given in
140 Section 5.

141

142

143 **2 Materials and Methods**

144 **2.1 Study area description**

145 West Africa covers about one-fifth of the African continent, extending from the Atlantic coast
146 of Senegal (18°W) to eastern Chad (25°E) and from the Gulf of Guinea (4°N) to the Sahel
147 (25°N) (Figure 1). The region's climate is governed by the Inter-Tropical Convergence Zone
148 (ITCZ) or the Inter-Tropical Discontinuity (ITD), which represents the interface at the ground
149 between moist monsoon air and dry harmattan air with a migratory annual cycle (Pospichal et
150 al., 2010). The West African region features high climatic diversity (Vintrou, 2012), and covers
151 a wide range of ecosystems and bioclimatic regions (Nicholson, 2018). The latitudinal and
152 seasonal oscillation of the Inter-ITCZ divides the region into three main climatic domains,
153 namely the Sahel, Sudanian and Guinean zones (Sule & Odekunle, 2016). The Sahel zone is a
154 semi-arid region with a short rainy season and an annual average rainfall not exceeding 600
155 mm (Figure 1). This domain is highly vulnerable to the adverse effects of climate change (Tian
156 et al., 2023). The Sudanian zone stretches as a broad belt south of the Sahel, receiving an
157 average rainfall of 600 to 1200 mm (Srivast et al., 2023). The Guinean zone, known for its



158 rugged terrain with steep slopes (Orange, 1990), receives abundant rainfall throughout the year,
159 with an annual average between 1200 and 2200 mm (ECOWREX, 2018). These three climate
160 zones are characterized by distinct vegetation (Biaou et al., 2023) and rainy season patterns.
161 The Sahelian and Sudanian domains share a unimodal rainfall pattern, while the Guinean zone
162 experiences a bimodal rainfall pattern of two rainy seasons, driven by the West African
163 Monsoon (Rodríguez-Fonseca et al., 2015; Nicholson, 2018). It is worth noting that nearly half
164 of Africa's continental watersheds are located in West Africa. The socioeconomic development
165 (agriculture, energy production, and livelihoods) of the region relies highly on the water
166 resources provided by these transboundary basins and aquifers (World Bank, 2021b).

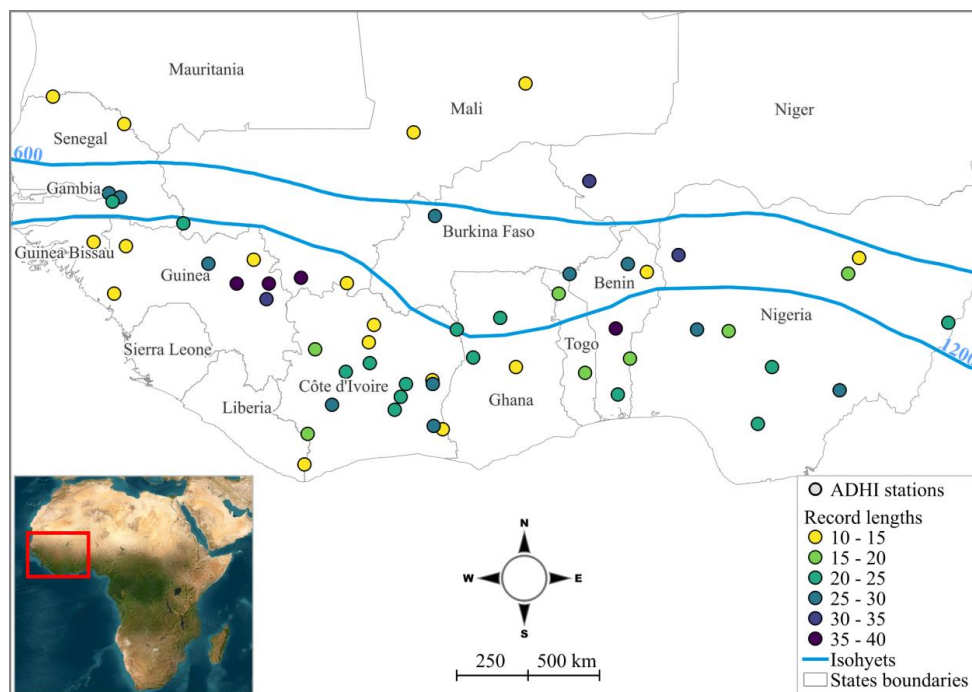
167

168

169 **2.2 Observational data**

170 Daily streamflow data for the period 1950-2018 were obtained from the African Database of
171 Hydrometric Indices (Tramblay et al. 2021b, Diop et al., 2025). This database provides
172 hydrometric indices computed from different data sources, with daily discharge time series that
173 span at least 10 years. In the ADHI database, the size of the 441 West African catchments
174 ranges from 95 to 2,150,000 km², and some stations have daily discharge data spanning over
175 44 years. Figure 1 shows the spatial distribution of the ADHI stations used in this study. We
176 only selected watersheds that met the following three criteria: (i) low regulation (see
177 Supplementary Figure S1), (ii) surface area of less than 150,000 km², and (iii) a daily
178 streamflow time series covering a minimum of 10 years between the 1950 and 2018.

179



180

181 Figure 1: Spatial distribution of the stations used in this study, covering the three climatic zones
182 in the West African region, as delimited by the blue isohyets (600 mm and 1200 mm annual
183 rainfall) on the map. The color of the circles indicates the record lengths of flood data (in years).
184 The blue lines represent isohyets delimiting West African climatic regions, and the white lines
185 indicate the borders of West African countries (African map from NASA 2005).

186

187 2.3 hydrological models

188 Two grid-based large-scale hydrological models were used to simulate river flows for the
189 period from 1950 to 2010: the HMF-WA model (the Hydrological Modelling Framework for
190 West Africa; Rameshwaran et al., 2021) and the Open Source (OS) LISFLOOD model (Van
191 Der Knijff et al., 2010), thereafter referred to as LISFLOOD. The HMF-WA model is adapted
192 from the modular HMF model, and enhanced by Rameshwaran et al. (2021) to include
193 additional key regional hydrological processes in the region such as wetlands, anthropogenic
194 water use, and endorheic rivers (Rameshwaran et al., 2021). The HMF-WA simulates spatially
195 consistent river flows across West Africa at a $0.1^\circ \times 0.1^\circ$ spatial resolution. Although the HMF-
196 WA model has not yet been specifically calibrated to individual West African catchments using
197 observed flow data where the model hydrology is configured to local conditions using spatial
198 datasets of physical and soil properties, its evaluation against observational data indicates that



199 it performs reasonably well in simulating both daily high and low river flows across most
200 catchments. The median values of NSE (Nash-Sutcliffe efficiency), NSE_{\log} and BIAS are 0.62,
201 0.82 and 0.06 (6 %), respectively (Rameshwaran et al., 2021). The LISFLOOD model is
202 developed at the Joint Research Centre (JRC) of the European Commission ([https://ec-](https://ec-jrc.github.io/lisflood/)
203 [jrc.github.io/lisflood/](https://ec-jrc.github.io/lisflood/)). LISFLOOD is a hybrid between a conceptual and fully physically based
204 distributed rainfall-runoff model, designed for simulating the hydrological processes that occur
205 in a catchment (Van Der Knijff et al., 2010). It supports a range of applications, including flood
206 forecasting, water resources management, and climate change impact assessments. The
207 LISFLOOD version used in this study (OS LISFLOOD v4.1.3) was calibrated using the
208 discharge stations data described in the previous section, with a 0.05° (~5 km) resolution in its
209 quasi-global implementation (-180, 180, 90, -60). This version of the LISFLOOD model, in
210 combination with the 0.05° implementation maps (v1.1.1 openly available from [https://global-](https://global-flood.emergency.copernicus.eu/)
211 [flood.emergency.copernicus.eu/](https://global-flood.emergency.copernicus.eu/)), has allowed the generation of the latest Copernicus
212 Emergency Management Service Global Flood Awareness System (CEMS GloFAS v4.0;
213 <https://www.globalfloods.eu/>) reanalysis and forecast datasets.

214

215 **2.4 Bias-corrected CMIP6 models and scenarios**

216 The sixth phase of the Coupled Model Intercomparison Project (CMIP6) provides simulations
217 from GCMs for the preindustrial period (1850–2014) and future climate projections (2015–
218 2100) (Noël et al., 2022). To assess future climate impacts on floods, we have used five (5)
219 daily GCMs rainfall and temperature outputs from the CMIP6 experiments ([https://esgf-](https://esgf-node.llnl.gov/search/cmip6)
220 [node.llnl.gov/search/cmip6](https://esgf-node.llnl.gov/search/cmip6)). Table 1 gives the institute name and references of the CMIP6
221 climate models used in this study. These GCMs encompass a range of climate sensitivities,
222 with Equilibrium Climate Sensitivity (ECS) values ranging from 2.98 to 5.34 (IPCC, 2021).
223 The GCMs were selected based on their availability for the study area. Due to their
224 accessibility, these GCMs have been widely used for climate impact assessments in Africa
225 (Dosio et al., 2019; Almazroui et al., 2020; Klutse et al., 2021; Babaousmail et al., 2023; Noon
226 et al., 2023). The Cumulative Distribution Function-transform (CDF-t) (Michelangeli et al.,
227 2009) was used to bias-correct the GCMs outputs. The CDF-t approach involves mapping the
228 cumulative distribution function (CDF) from a GCM in the historical period to the observed
229 CDF, then applying the same mapping to the GCM's future CDF (Flaounas et al., 2013; Pierce
230 et al., 2015; Famien et al., 2018). The CDF-t method requires high-resolution observational
231 data to work properly. The EWEMBI dataset (E2OBS, WFDEI, and ERA-I data, bias-corrected



232 for ISIMIP; Frieler et al., 2017; Lange, 2018, 2019) was used to bias-correct the climate
233 variables to drive the HMF-WA hydrological model. Similarly, the ERA5-land reanalysis
234 (Muñoz-Sabater et al., 2021). was used for bias-correcting the GCMs outputs for the
235 LISFLOOD model. The bias-corrected simulations are post-processed onto the $0.1^\circ \times 0.1^\circ$ (~10
236 km x 10 km) HMF-WA model grid (Rameshwaran et al., 2021, 2022), and onto the $0.05^\circ \times$
237 0.05° (~5 km x 5 km) LISFLOOD model grid for the period 1950-2100. CMIP6 models use
238 five Shared Socioeconomic Pathways (SSPs). SSPs are an updated framework of climate
239 scenarios, building upon the CMIP5 Representative Concentration Pathways (RCPs) while
240 maintaining consistency in the 2100 radiative forcing levels. SSPs describe the socioeconomic
241 factors (population growth, economic development, technological advancements, and
242 governance) which can influence greenhouse gas emissions and adaptation strategies (O'Neill
243 et al., 2017). Two Shared Socioeconomic Pathways (SSPs) are analysed in this study: the SSP2-
244 4.5 (Middle of the Road) and the SSP5-8.5 (Fossil-Fueled Development).

245 **Table 1:** Bias-corrected CMIP6 climate models used in this study

Institute	Climate Model	References
Max Planck Institute for Meteorology (Germany)	MPI-ESM1-2-HR	(Mauritsen et al., 2019)
Meteorological Research Institute (Japan)	MRI-ESM2-0	(Yukimoto et al., 2019)
Institute Pierre-Simon Laplace (France)	IPSL-CM6A-LR	(Boucher et al., 2020)
Met Office Hadley Centre (UK)	UKESM1-0-LL	(Mulcahy et al., 2020)
Geophysical Fluid Dynamics Laboratory (USA)	GFDL-ESM4	(Dunne et al., 2020)

246

247 **2.5 Evaluation of hydrological models**

248 The two hydrological models are evaluated over the period 1950-2014, which represents a
249 compromise between the period covered by the ADHI database and the historical CMIP6 GCM
250 simulations. To achieve this, we use the two-sample Anderson-Darling (AD) test at the 0.05
251 significance level (Scholz & Stephens, 1986) to compare the distributions of extreme values
252 observed and simulated by the hydrological models. The Block-Maxima approach (Gumbel,
253 1958) is used to construct extreme value time series, by extracting the annual maximum flow
254 (AMF) from the daily discharge time series over the period 1950-2014. Unlike the
255 Kolmogorov-Smirnov (KS) test (Berger & Zhou, 2014), which measures the maximum



256 distance between two cumulative distribution functions (CDFs), the AD test assesses the
257 overall distance between these CDFs, giving more weight to the tails of distributions. As a
258 result, the AD test is more sensitive than the KS test in the tails of distributions and is therefore
259 more suitable for comparing extreme values distributions (Engmann & Cousineau, 2011). That
260 said, the AD test also has a limitation as the reliability of an empirical CDF can be affected by
261 small sample sizes, particularly in the tails of the distribution. The performance of each
262 hydrological model is given here by the proportion of CMIP6 simulations (among the 5) for
263 which the AD test has failed.

264

265 **2.6 Extremes Values Analysis Framework**

266 **2.6.1 The Generalized Extreme Value Distribution**

267 According to the theory of extreme values, based on the Fisher–Tippett theorem, the
268 Generalized Extreme Value (GEV) is the limiting distribution of independent and identically
269 distributed random variables (Coles, 2001). The GEV is among the most frequently used
270 distributions for extreme value analysis. It is a continuous three-parameter distribution that can
271 account for non-stationarity, which refers to changes in statistical properties over time. This is
272 achieved by allowing the parameters to vary as a function of time or other covariates (Hamdi
273 et al., 2018; Wilcox et al., 2018). We, therefore, used the GEV to model the AMF series from
274 each hydrological model simulations forced with the five CMIP6 climate models at each
275 catchment. There are three parameters (location, scale and shape) in the GEV distribution
276 (Hossain et al., 2021). In flood frequency analysis, each GEV parameter plays a distinct role in
277 understanding and projecting flood behaviour, thus guiding effective flood risk management
278 (Lawrence, 2020). The location parameter (μ) indicates the central tendency of flood
279 magnitudes, with higher values suggesting a shift towards more frequent or severe floods. The
280 scale parameter (σ) measures the variability or dispersion of the distribution, with larger values
281 indicating greater uncertainty and a broader range of flood magnitudes. The shape parameter
282 (ξ) governs the tail behaviour of the distribution, with heavier tails suggesting an increased
283 probability of extreme flooding events. This parameter is crucial for assessing the risk of rare
284 floods and informing the design infrastructure to withstand such extremes. Equation (1)
285 presents the cumulative distribution function (CDF) of the GEV (Coles, 2001).



$$F(x; u, \alpha, \xi) = \exp\left\{-\left[1 - \xi \frac{(x-u)}{\alpha}\right]^{1/\xi}\right\} \quad \kappa \neq 0$$
$$F(x; \xi, \alpha) = \exp\left\{-\exp\left[-\frac{(x-u)}{\alpha}\right]\right\} \quad \kappa = 0$$
(1)

286

287 Where x , u , α , et ξ are the data, location, scale, and shape parameters respectively, and $(u +$
288 $\alpha/\xi) \leq x < \infty$ if $\xi < 0$; $-\infty < x < \infty$ if $\xi = 0$; $-\infty < x \leq (u + \alpha/\xi)$ if $\kappa > 0$.

289

290 Efficiently estimating the GEV parameters is crucial for the precise characterization and
291 analysis of extreme events (Rai et al., 2024). We have used the Generalized (Penalized)
292 Maximum Likelihood Estimation (GMLE) method (Martins & Stedinger, 2000) to estimate the
293 GEV parameters in a non-stationary context. The GMLE method overcomes the limitations of
294 the well-known MLE (Fisher, 1992) method for small sample size (Hossain et al., 2021). To
295 achieve this, Martins & Stedinger (2000) used a beta distribution (with shape parameters $p = 6$
296 and $q = 9$) as a prior to constraint the values of the GEV shape parameter in the interval $[-0.5,$
297 $+0.5]$, avoiding large negative values of the shape parameter. This approach has been used in
298 several studies to estimate the GEV parameters in both stationary and non-stationary contexts
299 (El Adlouni et al., 2007; Panthou et al., 2013; Trambly et al., 2024). However, the original
300 prior distribution from Martins & Stedinger (2000) is not well-suited for West Africa, as it
301 results in shape parameter estimates below -0.5 for several stations, as illustrated in
302 Supplementary Figure S2. Here, we therefore use a normal distribution as a prior for the GMLE
303 method. This normal distribution is fitted to the GEV shape parameter values estimated on 98
304 AMF series spanning a minimum of 20 years over the period 1950-2018 from the ADHI
305 database Trambly et al. (2021) using the L-moments method (Hosking, 1990). The newly
306 developed regional prior, modelled as a normal distribution, has a mean of -0.24 and a standard
307 deviation of 0.16 (see Supplementary Figure S2).

308

309

310 **2.6.2 Determining magnitude and direction of changes in flood events**

311 To analyse future changes in floods, we compare two 30-year future periods (a near-term future
312 [2031–2060] and a long-term future [2071–2100]) to a reference historical period (1985-2014)
313 at stations where there is a good fit between observed (OBS) AMF series and hydrological
314 models simulations (HIST) according to the Anderson-Darling (AD) test (at 0.05 level), and



315 also in stations at which the null hypothesis of the AD test is rejected. We have chosen to work
316 with the 2-year and 20-year floods to analyse the impacts of climate change in West Africa.
317 The 2-year return period indicates relatively frequent flood events, and this information is
318 essential for understanding and managing risks associated with flooding. The 20-year flood
319 event is frequently used for comparative purposes in various studies, as it balances the rarity of
320 extreme events (data length limitations) and the uncertainty in the estimated return levels
321 (Dawson et al., 2005; Trambly & Somot, 2018; Han et al., 2022). Thus, the 2- and 20-year flood
322 quantiles are computed at each station for the three 30-year periods using the GEV model fitted
323 to the AMF series by the GMLE method. Changes in flood are quantified in this study by
324 computing the ratio of the difference between the future flood quantile (Q_{future}) and the
325 historical flood quantile (Q_{hist}) to Q_{hist} itself. To assess the statistical significance of the
326 differences between the historical and future flood quantiles, we have used the parametric
327 bootstrapping approach. After estimating the GEV distribution parameters, we have generated
328 2500 simulations of annual peak floods for each subperiod (with each simulation representing
329 a sample of 30 data points). We have then recomputed the 2-year and 20-year flood quantiles
330 for each simulation. The significance of the differences between the quantiles was evaluated at
331 the 0.05 level. It is crucial to consider the degree of consensus among multiple climate models
332 to reduce the potential noise in the projections and reach robust conclusions (Awotwi et al., 2021;
333 Dosio et al., 2021). Here we have computed a multi-model index of agreement (MIA) as
334 introduced by Trambly & Somot (2018), to present the results in terms of the proportion of
335 CMIP6 models projecting significant change for each station. The MIA allows the assessment
336 of the robustness of climate model projections, ensuring cross-catchment comparability due to
337 its standardised scale ranging from -1 to 1, according to the direction of change (i.e., $MIA = 1$
338 (-1) if all models project an increasing (decreasing) trend).

339
$$MIA = \frac{1}{n} (\sum_{m=1}^n i_m) \quad (2)$$

340 From equation (6), for a given CMIP6 model (m), $i_m = 1$ for regionally significant upward
341 trends, $i_m = -1$ for significant negative trends, and $i_m = 0$ when no significant trends are
342 detected, across n climate simulations.

343

344 **2.6.3 Determining temporal functions for GEV parameters and modelling of non-**
345 **stationary extreme values**



346 While the previous section focused on the magnitude and direction of changes in flood events
347 under different scenarios, this section describes the methodology used to identify when these
348 changes began. Understanding how the parameters of the GEV distribution might shift under
349 future climate scenarios is a critical question that needs to be addressed given the accelerating
350 impacts of global warming on environmental conditions. Answering this question can inform
351 a more reliable modelling process to estimate flood quantiles. Several studies have suggested
352 that both the location and scale parameters of the GEV distribution should be adjusted
353 proportionally to account for the effects of climate change (Stedinger & Griffis, 2011;
354 Prosdocimi & Kjeldsen, 2021; Jayaweera et al., 2024). Here, to determine the appropriate
355 temporal function for the non-stationary GEV, the trends in GEV parameters are detected using
356 the non-parametric Mann-Kendall test (Mann, 1945; Kendall, 1975). As the test is applied to
357 parameters estimated over moving windows, it is important to note that temporal correlation is
358 introduced, which can bias the results of the original Mann-Kendall test, as it assumes
359 independence of observations. To address this, we have applied a modified version of the test
360 based on the Hamed & Rao (1998) variance correction approach, specifically adapted for
361 serially correlated data. A window size of 30 years has been selected to ensure sufficient data
362 to fit the SGEV, with a total of 121 windows. For each window, each hydrological model
363 (LISFLOOD and HMF-WA) and each climate scenario (SSP2-4.5 and SSP5.8-5), the SGEV
364 is fitted to AMF series from the averaged hydrological simulations driven by data from the
365 CMIP6 models. The Mann-Kendall test is then applied to the series of estimated parameters at
366 the 0.05 significance level.

367

368 Based on the results of the trend analysis of the GEV parameters, the location (μ) and scale (σ)
369 parameters are expressed as linear functions of time, denoted as $\mu(t)$ and $\sigma(t)$, while the shape
370 parameter remains constant. Thus, the non-stationary GEV model involves a vector
371 $\psi = [\mu_0; \mu_1; \sigma_0; \sigma_1; \xi]$ of five unknown parameters. We have decided to keep the shape parameters
372 constant because it is uncommon for researchers to model all three GEV parameters as
373 covariate-dependent functions. Indeed, adding this level of complexity can significantly
374 complicate the model parameters estimation, particularly the shape parameter (Katz, 2013;
375 Papalexiou & Koutsoyiannis, 2013). Allowing any starting date (year t_0) of a possible
376 significant trend in the GEV location and scale parameter, we have considered three cases of
377 the non-stationary GEV (NSGEV; cf. Equations 3-5):

378



- 379 • Case 1 (GEV1): a linear trend with no breakpoint (i.e., a single trend over the entire
380 record for both the location and scale parameters):

$$\mu(t) = \mu_0 + \mu_1 t ; \sigma(t) = \sigma_0 + \sigma_1 t \quad \text{for } t \leq t_0 \quad (3)$$

- 381 • Case 2 (GEV2): a linear trend after a breakpoint (i.e., the location and scale parameters
382 are constant before the year t_0 and linearly dependent on time after t_0):
383

$$\begin{aligned} \mu(t) = \mu_0 ; \sigma(t) = \sigma_0 & \quad \text{for } t \leq t_0 \\ \mu(t) = \mu_0 + \mu_1(t-t_0) ; \sigma(t) = \sigma_0 + \sigma_1(t-t_0) & \quad \text{for } t \geq t_0 \end{aligned} \quad (4)$$

- 384 • Case 3 (GEV3): both trends before and after a breakpoint are considered (i.e., a linear
385 trend before and after year t_0 for both location and scale parameters):
386

$$\begin{aligned} \mu(t) = \mu_0 + \mu_1(t_0-t) ; \sigma(t) = \sigma_0 + \sigma_1(t_0-t) & \quad \text{for } t \leq t_0 \\ \mu(t) = \mu_0 + \mu_1(t-t_0) ; \sigma(t) = \sigma_0 + \sigma_1(t-t_0) & \quad \text{for } t \geq t_0 \end{aligned} \quad (5)$$

387
388 Unlike in Wilcox et al. (2018), where breakpoints are defined independently for $\mu(t)$ and $\sigma(t)$,
389 in the present study, we assume a common breakpoint for both parameters. This means that
390 both $\mu(t)$ and $\sigma(t)$ change simultaneously at the same point in time. To ensure that the NSGEV
391 model is fitted with sufficient data, the first start year is set no earlier than 20 years after the
392 beginning of the time series (1950) and the last start year is set no later than 20 years before
393 the end of the time series (2100). Thus, the possible starting years of change (t_0) fall between
394 1970 and 2070. There are as many NSGEV models as there are breakpoints or starting years,
395 and the non-stationary model with the highest log-likelihood is selected (see Supplementary
396 Figure S3). The procedure described above is inspired by several studies that focused on
397 detecting trends in hydroclimatic time series using non-stationary GEV (Hawkins & Sutton,
398 2012; Panthou et al., 2013; Blanchet et al., 2018; Hamdi et al., 2018; Trambly & Somot, 2018;
399 Wilcox et al., 2018).

400
401 Once the best breakpoint has been determined for each time-varying GEV model based on the
402 log-likelihood profile, the trend models (GEV1, GEV2 and GEV3) are compared with each
403 other using the Akaike information criterion (AIC; Akaike, 1974). The AIC criterion is widely
404 used to compare multiple statistical models by assessing their goodness-of-fit. It accounts for
405 the trade-off between a model's fit to the data and its complexity, by penalising for more
406 complex models. While a more complex model may provide a better fit, it often does not



407 provide sufficient improvement to justify the addition of extra parameters (Wilcox et al., 2018).
408 Thus, the AIC is well-suited for evaluating the performance of non-stationary GEV models.
409 Furthermore, a deviance test (D) based on likelihood ratio (LR; Coles, 2001) is performed at
410 the 0.05 significance level between the best GEV trend model selected previously based on the
411 AIC criterion and the stationary GEV model (SGEV). The LR test allows us to determine the
412 best model between two competing nested models by comparing the D-statistic given by
413 Equation (6) to the chi-square (χ^2) distribution.

$$414 \quad D = 2\{\log(\text{ML}_{\text{NSGEV}}) - \log(\text{ML}_{\text{SGEV}})\} \quad (6)$$

415 From Equation (6), D represents the deviance test statistic value (referred to as D-statistic
416 above), $\log(\text{ML}_{\text{NSGEV}})$ and $\log(\text{ML}_{\text{SGEV}})$ are the maximised log-likelihood functions of the
417 NSGEV and the SGEV, respectively. Letting c_α be the $(1 - \alpha)$ quantile of the chi-square
418 distribution (where α represents the level of significance), with ν degrees of freedom equal to
419 the difference in the number of model parameters between the non-stationary and stationary
420 models, the non-stationary GEV is accepted at the level α if the D-statistic is greater than c_α ,
421 meaning a significant trend in the data.

422 To reduce Type 1 errors (Mudge et al., 2012) that could arise from the deviance test based on
423 the likelihood ratio and assess the field significance of the detected local trends, the False
424 Discovery Rate (FDR) procedure is implemented (Hochberg & Benjamini, 1995). The FDR
425 procedure aims to reduce the proportion of false positives among the null hypothesis local
426 rejections by adjusting the vector of p-values from the set of at-site tests (Wilks, 2006). The
427 FDR approach has been used in many studies of hydroclimatic variables due to its advantages
428 over other methods, such as dealing with spatial autocorrelation (Khaliq et al., 2009). For
429 consistency with local deviance and MK tests, the FDR procedure is computed at 0.05 global
430 significance level (α_{global}). The FDR test rejects the local null hypothesis when the
431 corresponding p-value is lower than α_{global} . If the null hypothesis is rejected at least once within
432 the study area, field significance is then declared (Wilks, 2016).

433

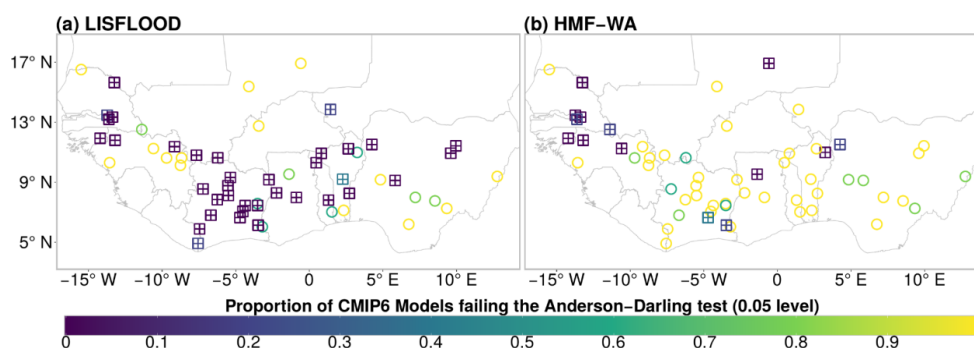
434

435 **3 Results and discussions**

436 **3.1 Assessing the performance of hydrological models**



437 The two hydrological models' performance is assessed over the period 1950-2014 by applying
438 the two-sample Anderson-Darling (AD). The results of the statistical evaluation of the two
439 hydrological models are shown in Figure 2. The performance of each model at each station is
440 assessed based on the proportion of CMIP6 models that fail the Anderson-Darling test at the
441 0.05 significance level. Specifically, if more than two out of five CMIP6 simulations fail the
442 test at a given station, the hydrological model is considered to perform poorly at that station.
443 Considering this evaluation criterion, the LISFLOOD hydrological model performs well at 64
444 % of the stations, while the HMF-WA model performs satisfactorily at only 24 % of the stations
445 (Figure 2). Although both models are semi-physically based and spatially distributed, the
446 LISFLOOD model outperforms the HMF-WA model in simulating extreme flows in West
447 Africa (Figure 2). This difference in performance can be attributed to several factors: (i) the
448 LISFLOOD model was run at a finer resolution ($0.05^\circ \times 0.05^\circ$) compared to the coarser
449 resolution of $0.1^\circ \times 0.1^\circ$ used by the HMF-WA model (Rameshwaran et al., 2021); (ii) the
450 HMF-WA model includes fewer meteorological forcings and only a limited number of
451 hydrological processes (specifically wetlands, anthropogenic water use, and endorheic rivers),
452 whereas the LISFLOOD model can incorporate over 70 different processes depending on the
453 target application (i.e., rainfall-runoff transformation, flood and drought forecasting) and the
454 required level of configuration (more detailed information on the configuration of LISFLOOD
455 can be found at <https://ec-jrc.github.io/lisflood-model>; and (iii) the HMF-WA model has not
456 been calibrated to individual west African catchment conditions with observed flow data
457 (Rameshwaran et al., 2021). In contrast, the LISFLOOD model, in its quasi-global
458 implementation, has been calibrated using in-situ discharge observations covering several river
459 basins worldwide, including most West African basins, and with discharge time series spanning
460 at least four years after 01 January 1980. Consequently, while the distributed nature of the
461 HMF-WA model aims to improve the understanding of regional climate change impacts in a
462 spatially coherent manner across West Africa, it does not necessarily lead to better modelling
463 of extreme flows in the various climates and socioeconomic contexts of the region without
464 calibration.

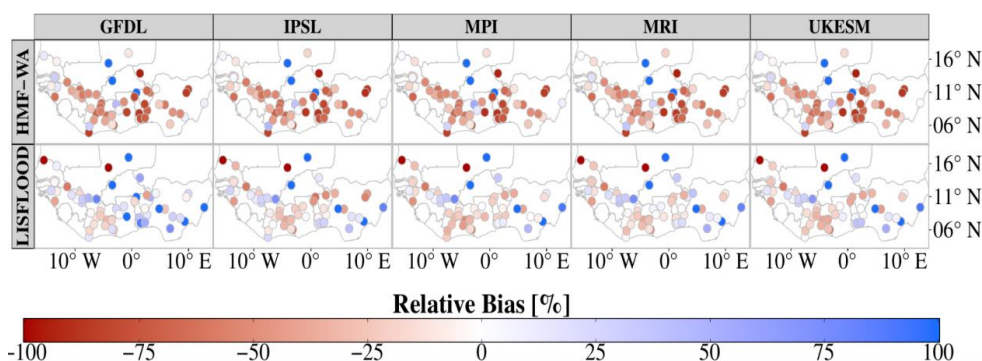


465
 466 Figure 2: Statistical evaluation of the two hydrological models: a) Two-sample Anderson-
 467 Darling (AD) goodness-of-fit (GOF) test at 0.05 statistical significance level at each station
 468 between the AMF of daily OBS from the ADHI database and annual maxima flow of HIST
 469 from LISFLOOD daily simulations forced with the five CMIP6 GCMs (GFDL, IPSL, MPI,
 470 MRI, and UKESM) over the period 1950-2014. b) same as a) but using HMF-WA as
 471 hydrological model. The Performance of each hydrological model is given by the proportion
 472 of CMIP6 simulations for which the AD test has failed. The circles show stations where 60-
 473 100 % of CMIP6 models fail the test, and squares represent stations where 0–20 % of CMIP6
 474 models fail the AD test.
 475

476 To further assess the performance of the hydrological models in capturing extreme flows, we
 477 computed the Relative Bias between the AMF simulated by the LISFLOOD-CMIP6 and HMF-
 478 WA-CMIP6 hydrological models and the observed AMF from the ADHI database. This
 479 comparison was performed over the historical period (1950–2014), focusing on the
 480 climatological characteristics of AMF (median values) rather than on year-to-year
 481 correspondence. This approach allows us to evaluate whether the hydrological models tend to
 482 overestimate or underestimate flood peaks, considering climate models individually. As shown
 483 in Figure 3, the HMF-WA model consistently shows a negative relative bias across all GCMs,
 484 with median values ranging from -52 % (IPSL) to -46 % (UKESM) across the region. These
 485 negative biases suggest a tendency of the HMF-WA model to underestimate peak flow. The
 486 LISFLOOD model, in contrast, shows lower bias than the HMF-WA model, with a mix of
 487 slight underestimations and even overestimations (Figure 3). For instance, the median values
 488 for the LISFLOOD model simulations range from -14 % (MPI) to 7 % (GFDL). Although the
 489 LISFLOOD model also shows negative biases with most GCMs, such as IPSL, MPI, MRI, and
 490 UKESM, the magnitude of these biases is much smaller compared to the HMF-WA model.
 491 Nevertheless, whether a calibrated hydrological model offers more reliable climate change
 492 projections than an uncalibrated model, which may perform less accurately in reproducing
 493 historical conditions (Pechlivanidis et al., 2017), remains questionable. Examining whether



494 their capacity to simulate hydrological responses to historical climate is influencing projected
 495 trends for climate change impacts remain important, especially considering that most
 496 projections of climate change impacts on African hydrological trends were produced using
 497 uncalibrated models (Davie et al., 2013; Sauer et al., 2021).



498
 499 Figure 3: Relative bias (percentages) computed between simulated AMF from LISFLOOD-
 500 CMIP6 and HMF-WA-CMIP6 hydrological models' simulations, and observed AMF from the
 501 ADHI database, for the historical period (1950-2014).

502

503 3.2 Magnitude and direction of changes in flood events

504 To analyse changes in floods, we have compared two 30-year future periods (a near-term future
 505 [2031–2060] and a long-term future [2071–2100]) to a reference historical period (1985-2014).
 506 To achieve this, we have fitted the GEV distribution the AMF series of each model simulation
 507 using the GMLE method. Then, the 2- and 20-year flood quantiles are computed at each station
 508 for the three 30-year periods. Figure 4 shows the MIA on the direction of changes in the 2-year
 509 and 20-year floods for the near-term and long-term futures, from both LISFLOOD and HMF-
 510 WA models simulations under SSP2.4-5 and SSP5.8-5 scenarios. Despite their differences in
 511 terms of hydrological processes representation (model structures) and input data, the two
 512 hydrological models generally projected consistent impacts of climate change on future floods
 513 across the West African region. Both hydrological models consistently project an increase
 514 (positive change) in floods in the near-term and long-term futures across West Africa (Figure
 515 4).

516 In the near-term future (2031–2060), there is a high level of agreement in projecting positive
 517 changes in the 2-year flood event under both SSP2-4.5 and SSP5-8.5 scenarios. The



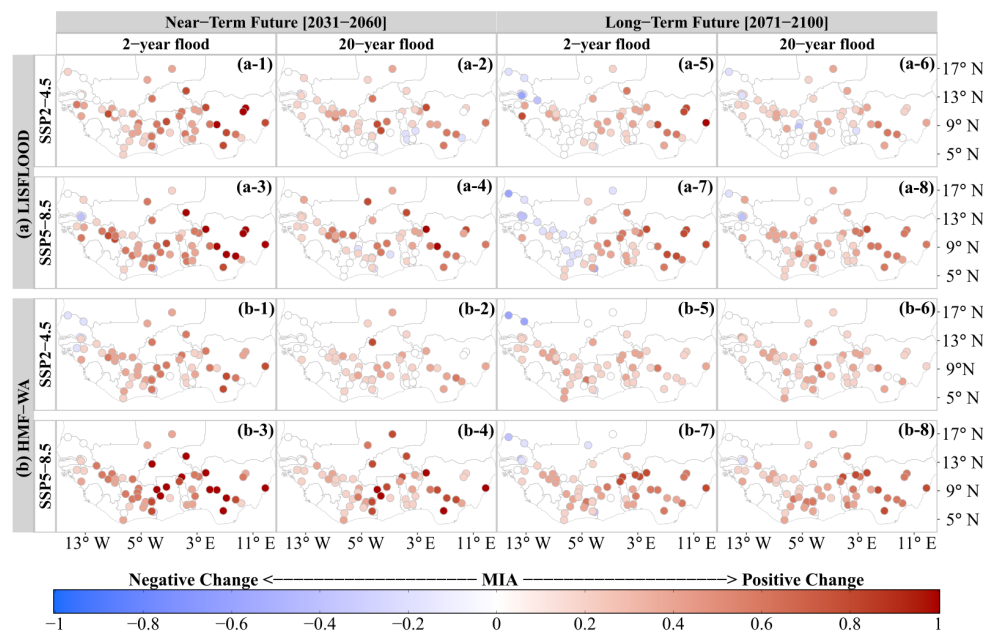
518 simulations of the LISFLOOD and HMF-WA models show strong agreement across the
519 CMIP6 models. Under SSP2-4.5, the MIA values range from -0.2 to 1 for the LISFLOOD
520 model (Figure 4a-1), and from -0.2 to 0.8 for the HMF-WA model (Figure 4b-1). This
521 agreement increases for both hydrological models under SSP5-8.5, with MIA values falling
522 between -0.2 and 1 for both LISFLOOD (Figure 4a-3) and HMF-WA models (Figure 4b-3).
523 The consistent climate change impact projections suggest that more frequent flood events are
524 expected to become increasingly common across the West African region. For the 20-year
525 flood event, which is less frequent but more severe, MIA values range from -0.2 to 0.8 (-0.2 to
526 1) and from 0 to 0.8 (0 to 1) under the SSP2-4.5 (SSP5-8.5) for the LISFLOOD (Figure 4a-2
527 and Figure 4a-4) and HMF-WA (Figure 4b-2 and Figure 4b-4) models, respectively.

528

529 In the long-term future (2071–2100), considering the 2-year flood, MIA values range from -
530 0.6 to 1 (-0.6 to 0.8) and from -0.6 to 0.6 (0.4 to 0.8) under the SSP2-4.5 (SSP5-8.5) for the
531 LISFLOOD (Figure 4a-5 and Figure 4a-7) and HMF-WA (Figure 4b-5 and Figure 4b-7)
532 models, respectively. For the 20-year flood, model agreement in projecting the positive changes
533 in flood magnitude remains relatively high, with MIA values ranging from -0.4 to 0.6 (-0.4 to
534 0.8) and from 0 to 0.6 (-0.2 to 0.8) under the SSP2-4.5 (SSP5-8.5) for the LISFLOOD (Figure
535 4a-6 and Figure 4a-8) and HMF-WA (Figure 4b-6 and Figure 4b-8) models, respectively. It is
536 also worth noting that negative changes are projected in the 2-year flood in the long-term future
537 in a few sets of catchments located in the western part of the region (Figure 4a-5, 4a-7, 4b-5
538 and 4b-7). This area is also projected to experience a decrease in annual rainfall when looking
539 at the full CMIP6 ensemble (IPCC, 2021). However, the agreement between the CMIP6 models
540 remains very weak, indicating a lower confidence in the robustness of these negative changes
541 compared to the regional pattern. Overall, the agreement between the CMIP6 and the
542 hydrological models is higher for the near-future than for the long-term future, reflecting
543 increased uncertainty as the projection timeline extends.

544

545



546

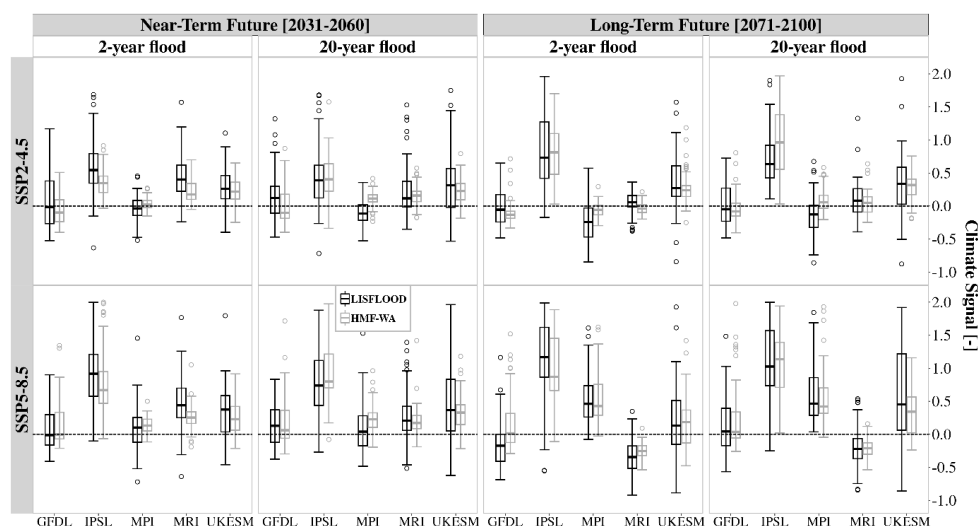
547 Figure 4: Spatial distribution of the multi-model index of agreement (MIA) on the direction of
 548 changes in 2-year and 20-year flood events for the near-term (2031-2060) and long-term (2071-
 549 2100) futures, compared to the historical reference period (1985-2014). This analysis combines
 550 simulations from: (a) LISFLOOD and (b) HMF-WA hydrological models, forced with five
 551 bias-corrected CMIP6 models (GFDL, IPSL, MPI, MRI, and UKESM), under the SSP2.4-5
 552 (a1 to a4 and b1 to b4) and SSP5.8-5 (a5 to a8 and b5 to b8) scenarios. Flood quantiles are
 553 estimated using the GEV distribution fitted with the GMLE method. Negative change (decrease
 554 in flood quantiles) is represented by shades of blue, and positive change (increase in flood
 555 quantiles) is represented by shades of red.

556

557 Figure 5 summarises the projected climate impacts on floods in the near-term (2031-2060) and
 558 long-term (2071-2100) futures in West Africa across the different CMIP6 models (GFDL,
 559 IPSL, MPI, MRI, and UKESM). Both hydrological models' simulations consistently suggest
 560 strong changes in floods, with most median values falling above the zero-change baseline.
 561 Considering the CMIP6 models' projections individually in the near-future, under both
 562 SSP2-4.5 (Figure 5a) and SSP5-8.5 (Figure 5b) scenarios, the most pronounced changes are
 563 obtained for both hydrological models when forced with IPSL, MRI, and UKESM models.
 564 These near-term projections highlight the potential for more frequent extreme flood events,
 565 leading to increased flood risks and greater socioeconomic vulnerability in the West African
 566 region. In the long-term future, the distribution of flood trends is quite consistent between the
 567 two hydrological models, and the variability stems only from GCMs. For instance, under



568 SSP2-4.5, the variability between the different CMIP6 models is very pronounced, with most
 569 projections showing relatively modest changes compared to the SSP5-8.5 scenario, where most
 570 of the GCM agree for a positive change in floods magnitudes.



571

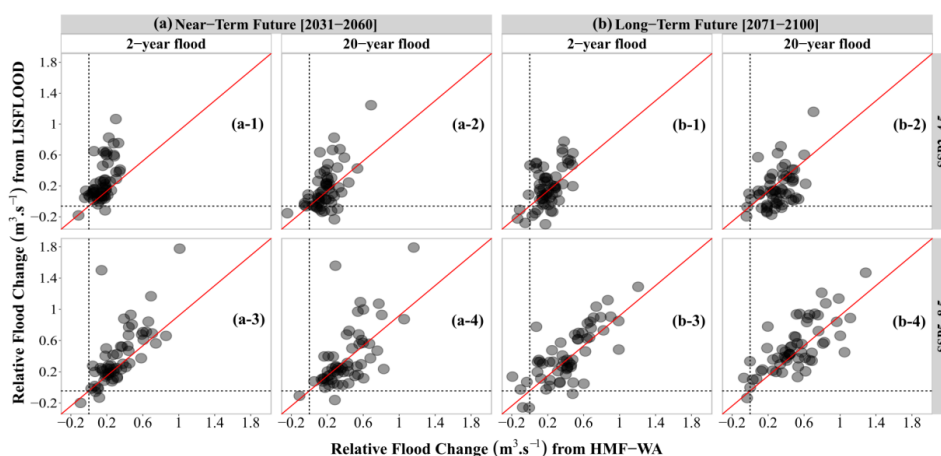
572 Figure 5: Synthesis of the projected changes in the 2-year and 20-year floods in West Africa
 573 from the LISFLOOD (black boxplots) and HMF-WA (grey boxplots) model simulations forced
 574 with the five CMIP6 GCMs (GFDL, IPSL, MPI, MRI, and UKESM), under both SSP2-4.5
 575 (top row) and SSP5-8.5 (bottom row) climate scenarios, for the near-term (2031-2060) and the
 576 long-term (2071-2100) futures. The black dotted line represents the zero-change baseline.

577

578 To further assess the agreement between the two hydrological models, Figure 6 shows the
 579 scatter plots illustrating how projected changes (Δ Flood) in floods compares between
 580 LISFLOOD and HMF-WA model simulations. Overall, both models project positive change
 581 in floods in West Africa regardless of the climate scenario considered. Indeed, most data points
 582 fall above the zero-change baseline, indicating a global positive change in floods from both
 583 hydrological model simulations (Figure 6). To confirm the agreement between the two models,
 584 we have computed the Spearman coefficient (ρ) between the projected multi model mean
 585 changes in floods (Δ Flood) from the simulations of the LISFLOOD and HMF-WA models.
 586 Supplementary Table S1 gives the Spearman coefficient (ρ) values for the 2-year and the 20-
 587 year floods, under the SSP2-4.5 and SSP5-8.5 scenarios. The correlation analysis shows that
 588 the agreement between the two models is particularly pronounced. under the SSP5-8.5
 589 scenario, suggesting a stronger influence of climatic changes under the high emissions



590 scenario. In the near-term future, the Spearman correlation coefficient is 0.75 (0.63) for the 2-
 591 year (20-year) floods. In the long-term future, the correlation remains high, with 0.71 (0.69)
 592 for the 2-year (20-year) floods, suggesting that the models continue to show strong agreement,
 593 even for long-term projections. These results indicate a relatively high level of consistency
 594 between the two hydrological models for projecting future flood changes, despite the
 595 systematic biases in HMF-WA model over the reference historical period. Thus, using both
 596 models, the climate forcing has more importance than the hydrological representation itself.

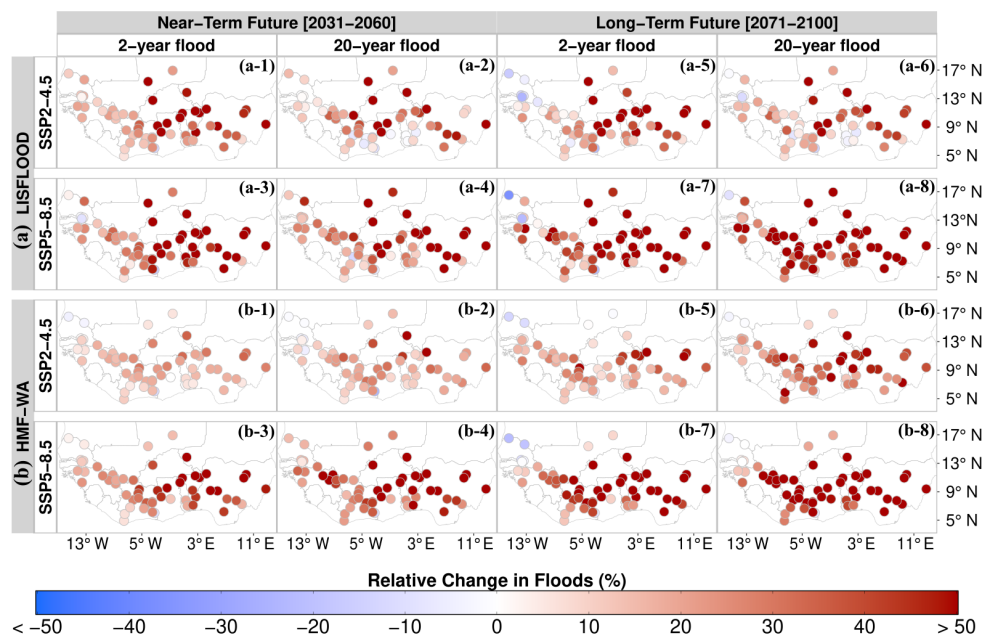


597
 598 Figure 6: Comparison of projected multi model mean changes in flood (Δ Flood) between
 599 LISFLOOD and HMF-WA hydrological models, under SSP2.4-5 and SSP5.8-5 scenarios, for
 600 the near-term (2031-2060) and the long-term futures (2071-2100), compared to the historical
 601 reference period (1985-2014). The gray dashed lines represent the zero-change baseline and
 602 the red diagonal line represents the theoretical 1:1 line where projected changes from both
 603 hydrological models would be identical.

604 The relative magnitude of change in floods was also analysed by computing the mean relative
 605 change. (i.e., ratio of the difference between the flood quantiles of the future periods and the
 606 reference historical period) across CMIP6 models for each hydrological model. The spatial
 607 distribution of the magnitude of changes, as simulated with the LISFLOOD and HMF-WA
 608 hydrological models under both SSP2-4.5 and SSP5-8.5, is shown in Figure 7a and Figure 7b,
 609 respectively. Supplementary Table S2 summarises the overall mean relative change in floods
 610 across the region from both hydrological model's simulations. The two hydrological models
 611 consistently project an increase in future floods across the West African region, with flood
 612 magnitudes at most sites exceeding 50 %, particularly under SSP5-8.5 (Figure 7a-3, 7a-4, 7a-



613 7, 7a-8, 7b-3, 7b-4, 7b-7, and 7b-8). These results are consistent with previous studies that
 614 argued for the ongoing rising trend in extreme streamflow across the West African catchments
 615 (Nka et al., 2015; Aich et al., 2016; Wilcox et al., 2018). Furthermore, the findings from the
 616 studies of Almazroui et al. (2020), Dosio et al. (2021) and Dotse et al. (2023) have shown that
 617 CMIP6 models contain a robust signal of the intensification of the rainfall regime in West
 618 Africa. The increasing trend in floods across the region may be partly explained by the trends
 619 in extreme precipitations, as their variability influences the hydrological dynamics of the region
 620 (Panthou et al., 2013; Wilcox et al., 2018; Elagib et al., 2021).



621

622 Figure 7: Mean relative changes in the 2-year and 20-year Floods in West Africa for Near-term
 623 (2031-2060) and Long-term (2071-2100) futures, based on simulations from the LISFLOOD
 624 (a-1 to a-8) and HMF-WA (b-1 to b-8) hydrological models, under SSP2-4.5 and SSP5-8.5
 625 scenarios.

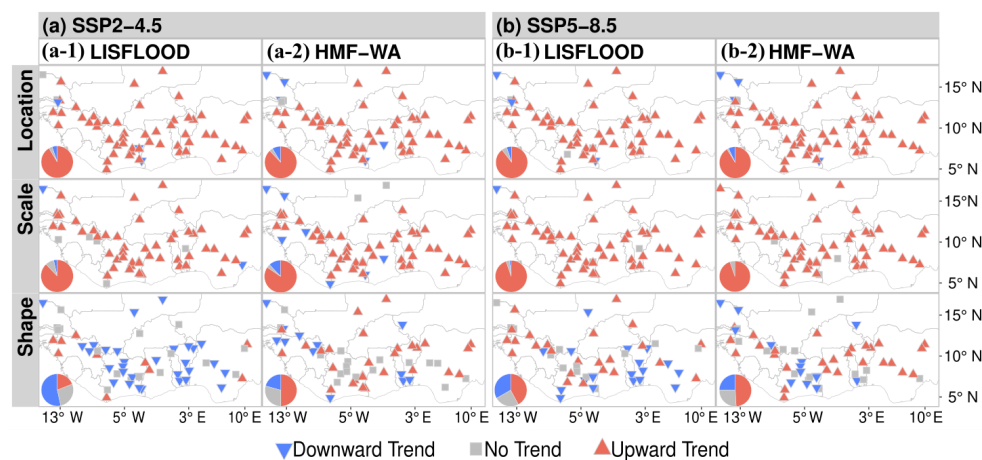
626

627 3.3 Onset of changes in AMF series

628 3.3.1 Observed trends in GEV Parameters



629 As the climate and environment change (Lee et al., 2023), it is essential to examine how these
 630 changes affect the parameters of GEV distributions. Figure 8 shows the spatial distribution of
 631 trends detected by the Mann-Kendall test on GEV parameters estimated on multi model mean
 632 streamflow over 30-year moving windows from 1950 to 2100. Both hydrological models
 633 project upward trends in the location and scale parameters across the West African region with
 634 a strong agreement between the two hydrological models (see Figure 8). All local trends are
 635 field significant at 0.05 level according to the FDR procedure. The simulated upward trends in
 636 both parameters, observed across various watersheds and emission scenarios, emphasize the
 637 importance of accounting for temporal variability in GEV parameters to reliably model future
 638 flood risks. An increase in the location parameter suggests more frequent and severe floods,
 639 while an upward trend in the scale parameter indicates greater variability in flood magnitudes.
 640 In contrast, the "mixed" trends observed in the shape parameter, with no distinct spatial
 641 patterns, support the decision to model it as constant over time, as there is no strong regional
 642 evidence of consistent temporal changes in its behaviour across the region.



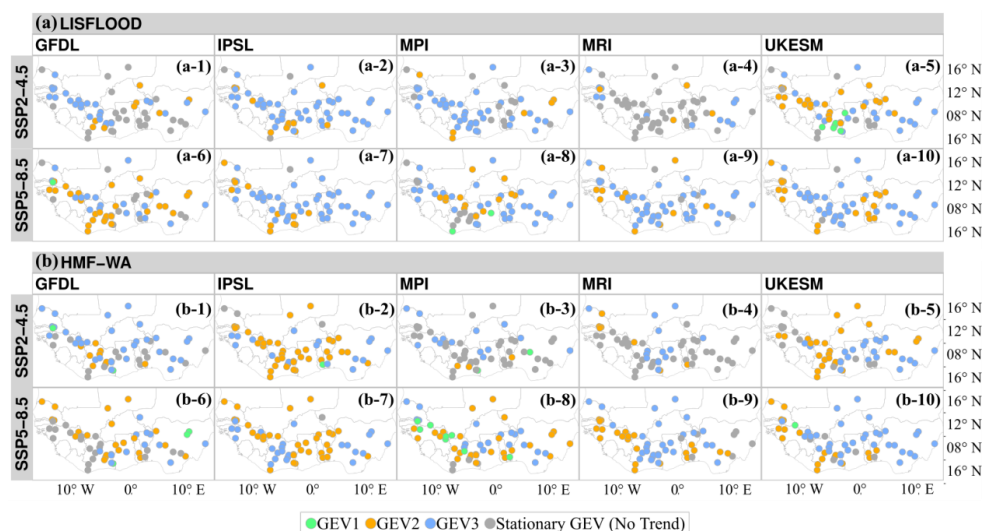
643
 644 Figure 8: Direction of significant trends detected using the Mann-Kendall trend test (at the 0.05
 645 significance level) for GEV parameters: location (top row), scale (middle row), and shape
 646 (bottom row). The GEV parameters are estimated based on multi-model mean streamflow over
 647 30-year moving windows. Panels (a-1) and (b-1) display the results for the LISFLOOD model
 648 under SSP2-4.5 and SSP5-8.5, respectively, while panels (a-2) and (b-2) show the results for
 649 the HMF-WA model under SSP2-4.5 and SSP5-8.5, respectively. The red upward triangles
 650 indicate significant upward trends, and the blue downward triangles indicate significant
 651 downward trends, both at the 0.05 significance level. Gray rectangles represent cases where no
 652 significant trends are detected. The pie charts summarize the proportion of stations showing
 653 significant positive trends (red), significant negative trends (blue), and non-significant trends
 654 (gray).



655 3.3.2 Selection of the best-suited GEV trend model

656 Using non-stationary GEV models, we analyse temporal shifts in floods by fitting
657 time-dependent GEV parameters to the AMF series from both hydrological model's
658 simulations. To detect the onset of significant trends in flood events, we have allowed any
659 starting year (t_0) of a possible trend in the GEV location $\mu(t)$ and scale $\sigma(t)$ parameter between
660 1970 and 2070. To select the best non-stationary GEV model for each site, we have compared
661 the goodness-of-fit of three different time-varying GEV models. The models evaluated are: (1)
662 a linear trend for both the $\mu(t)$ and $\sigma(t)$ parameters without a breakpoint (GEV1); (2) a linear
663 trend for $\mu(t)$ and $\sigma(t)$ starting after a specific breakpoint (GEV2); and (3) linear trends for $\mu(t)$
664 and $\sigma(t)$ both before and after a breakpoint (GEV3). Figure 9 shows the GEV trend model
665 selected at each station according to the AIC criterion and the deviance test for the
666 LISFLOOD-CMIP6 and HMFVA-CMIP6 simulations under both SSP2-4.5 and SSP2-8.5
667 scenarios. Although both hydrological models project an increase in floods (Figure 5), they
668 simulate slightly different trend patterns across the study area. Considering the LISFLOOD
669 model (Figure 9a), the GEV3 (double linear trend) is constantly best suited at most stations,
670 with a high agreement between the CMIP6 models. For instance, under the SSP2-4.5 scenario,
671 the GEV3 distribution outperforms other models at 66 %, 79 %, 76 %, when the LISFLOOD
672 model is driven by the GFDL (Figure 9a-1), IPSL (Figure 9a-2) and MPI (Figure 9a-3) climate
673 models, respectively. A similar trend is observed under the SSP2-8.5 where the GEV3 is best
674 suited when the LISFLOOD is forced with the MPI (62 %), MRI (77 %), IPSL (78 %), and
675 UKESM (66 %) models (Figure 9a-7, 9a-8, 9a-9 and 9a-10). The HMF-WA simulations show
676 a mixed spatial pattern between the GEV2 and GEV3 models (Figure 9b). For both
677 hydrological models, the single linear trend model (GEV1) is selected at very few stations (less
678 than 5 %). Meanwhile, the stationary behaviour observed at few sites under SSP2-4.5 suggests
679 that certain river basins may experience little to no change in their hydrological extremes under
680 moderate emissions pathways.

681



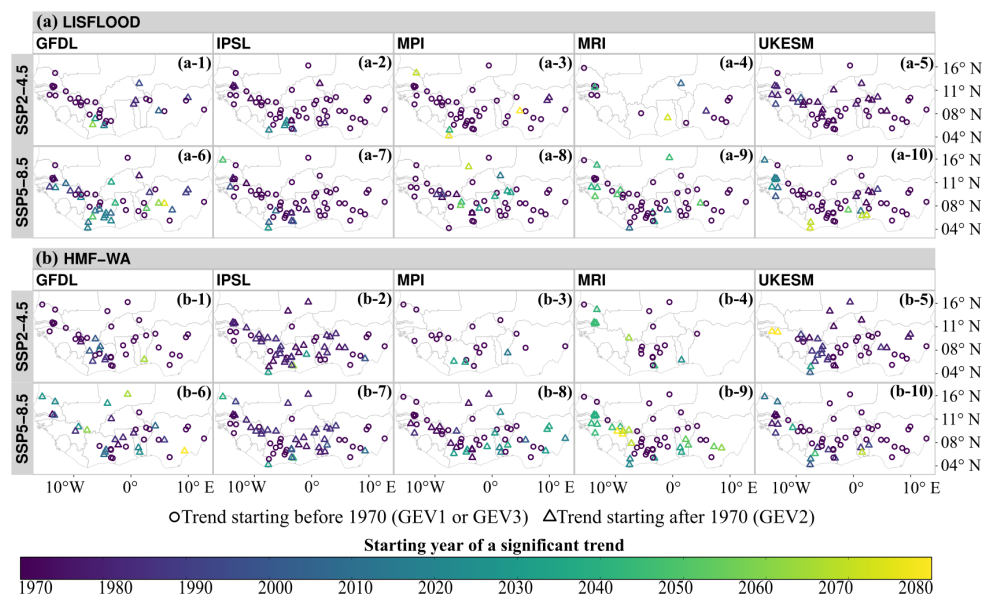
682

683 Figure 9: Best-fitting GEV trend models at each station, determined using the AIC criterion
 684 and the deviance test, based on simulations from (a) LISFLOOD-CMIP6 (top rows) and (b)
 685 HMF-WA-CMIP6 (bottom rows) simulations under SSP2-4.5 and SSP5-8.5 scenarios. The
 686 green points represent stations best modelled by GEV1, which assumes a linear trend over the
 687 entire record. The orange points indicate stations best modelled by GEV2, which assumes
 688 stationarity before a breakpoint followed by a linear trend after the breakpoint. The blue points
 689 denote stations best modelled by GEV3, which assumes a double linear trend. The grey points
 690 represent stations where all non-stationary GEV models are rejected based on the deviance test.

691

692 3.3.3 Starting years of trends in flood hazards

693 The spatial distribution of the starting years of significant flood trends detected with the GEV
 694 trend models are shown in Figure 10. The projections from the two hydrological models are
 695 spatially coherent, and the temporal variability on the start of flood trends in the region seems
 696 to depend on climate models. Overall, under both SSP2-4.5 and SSP5-8.5, the majority of
 697 significant trends are identified almost on the whole record, from the 1980s onward, in
 698 agreement with long-term trends observed in this region (Tramblay et al., 2020), particularly
 699 with the GFDL, IPSL, MPI, and UKESM models. This consistent pattern of early starting years
 700 suggests that West African communities are already facing high flood risks, and are likely to
 701 experience exacerbated conditions in the near-future.



702 Figure 10: Spatial distribution of the starting years of significant flood trends projected by (a)
 703 LISFLOOD and (b) HMF-WA hydrological models, forced with CMIP6 models (GFDL, IPSL,
 704 MPI, MRI, and UKESM), under SSP2-4.5 and SSP5-8.5 scenarios. The color gradient indicates
 705 the years of significant breakpoints in flood trends, ranging from 1970 (purple) to 2070
 706 (yellow). Circular markers represent sites where trends began at the start of the time series
 707 (before 1970). Triangular markers indicate sites where trends emerged after 1970 (the linear
 708 trend GEV2 case).
 709

710

711

712 Conclusions

713 This study has assessed the regional-scale hydrological impacts of climate change in West
 714 Africa, specifically focusing on floods, from two large-scale hydrological models (HMF-WA
 715 and LISFLOOD) driven by five bias-corrected CMIP6 climate models under SSP2-4.5 and
 716 SSP5-8.5 scenarios. A multi-model index of agreement (MIA) was used to assess the
 717 robustness of the projections from the hydrological model. The statistical evaluation of the two
 718 hydrological models, performed using the two-sample Anderson-Darling test between the
 719 annual maximum flows observed from the ADHI database and those simulated by the
 720 hydrological models, revealed that the LISFLOOD model outperforms the HMF-WA model in
 721 simulating extreme flows in West Africa. The GEV distribution was used to analyse trends and



722 detect change points by fitting and comparing multiple GEV models to the AMF series,
723 covering both the historical and future periods. Two 30-year future periods (a near-term future
724 [2031–2060] and a long-term future [2071–2100]) were compared to a reference historical
725 period (1985–2014). Despite differences in hydrological processes representation, model
726 architectures and calibration, the two hydrological models generally projected consistent
727 impacts of climate change on future floods across the West African region with a relatively
728 high level of consistency. This agreement between the two hydrological models suggests that
729 the climate forcing has more importance than the hydrological representation itself, and un-
730 calibrated models can provide reliable scenarios in this region. An increase in floods (2-year
731 and 20-year) is observed at more than 94 % of the stations, with some locations experiencing
732 flood magnitudes exceeding 45 %. The results of the comparison between GEV trend models
733 show that the double-linear trend GEV model with both location and scale parameters
734 expressed as time-dependent is the best suited for most stations. The analysis of the starting
735 years of significant flood trends revealed that most shifts in extreme flood patterns occurred
736 early in the time series, as early as the 1970s in several basins.

737

738 The use of the GCM outputs to drive hydrological models introduces uncertainties in
739 hydrological simulations. Indeed, the outputs of General Circulation Models (GCMs) are
740 characterised by uncertainties, arising from several factors such as the simplified representation
741 of complex Earth system interactions and atmospheric processes, the uncertain socioeconomic
742 pathways, the coarse spatial resolution of these models, along with challenges related to model
743 parameterization (Hawkins & Sutton, 2009). In addition, the performance of large-scale
744 hydrological models is influenced by the driving inputs, the representation of the hydrological
745 process, and the model parameterization (Andersson et al., 2015). Current models also have
746 difficulties in reproducing hydrological processes in arid regions (Heinicke et al., 2024). It
747 would therefore be interesting to explore in more details the main sources of uncertainties in
748 hydrological projections in West Africa to improve the realism of such modelling approaches
749 in the future.

750

751 **Code availability**



752 The codes used in this study are available upon request. The implementation of these codes
753 primarily relies on the R extRemes library (<https://www.jstatsoft.org/article/view/v072i08>).

754

755 **Data availability**

756 The ADHI dataset containing the observed annual maximum time series is available at:
757 <https://doi.org/10.23708/LXGXQ9>, and annual maximum dataset from the HMF-WA
758 simulations is available at: <https://doi.org/10.5285/346124fd-a0c6-490f-b5af-eaccbb26ab6b>.

759 The data that support the findings of this study are available from the corresponding author
760 upon reasonable request.

761

762 **Author contributions**

763 SBD, YT, and AB conceived and designed the study, with contributions from JE and BD. SBD,
764 YT, and JB developed the methodology. YT provided the ADHI dataset and parametric
765 bootstrapping code to assess the significance of flood trends. JE, BD, SG, and PS carried out
766 the LISFLOOD simulations. PR provided the HMF-WA model annual maximum flow dataset.
767 JB provided R code snippets to implement the GEV trend models. SBD performed the flood
768 frequency analysis and drafted the initial manuscript. YT and AB supervised the study. All
769 authors contributed to the writing and revision of the manuscript.

770

771 **Competing interest declaration**

772 The authors declare that they have no conflict of interest.

773

774 **Acknowledgements**

775 The PhD Grant of Serigne Bassirou Diop is funded by the AFD/IRD project CECC. The Phd
776 Grant of Job Ekolu is funded by the Centre for Agroecology Water and Resilience (CAWR) of
777 Coventry University, UK. The authors also extend their thanks to the various basin agencies in
778 West Africa for their contribution to data collection and Nathalie Rouche (SIEREM) for the
779 database management. Yves Trambly and Bastien Dieppois were supported by a PHC
780 ALLIANCE grant. Juliette Blanchet acknowledges receiving funding from Agence Nationale
781 de la Recherche - France 2030 as part of the PEPR TRACCS programme under grant number

<https://doi.org/10.5194/egusphere-2025-130>

Preprint. Discussion started: 4 March 2025

© Author(s) 2025. CC BY 4.0 License.



782 ANR-22-EXTR-0005. Ponnambalam Rameshwaran was supported by the Natural

783 Environment Research Council as part of the NC-International program (NE/X006247/1).

784



785 References

- 786 Agoungbome, S. M. D., Seidou, O., & Thiam, M. (2018). Evaluation and Update of Two Regional
787 Methods (ORSTOM and CIEH) for Estimations of Flow Used in Structural Design in West
788 Africa. In C. M. F. Kebe, A. Gueye, A. Ndiaye, & A. Garba (Eds.), *Innovations and*
789 *Interdisciplinary Solutions for Underserved Areas* (pp. 153–162). Springer International
790 Publishing. https://doi.org/10.1007/978-3-319-98878-8_15
- 791 Aich, V., Liersch, S., Vetter, T., Fournet, S., Andersson, J. C. M., Calmanti, S., van Weert, F. H. A.,
792 Hattermann, F. F., & Paton, E. N. (2016). Flood projections within the Niger River Basin under
793 future land use and climate change. *Science of The Total Environment*, 562, 666–677.
794 <https://doi.org/10.1016/j.scitotenv.2016.04.021>
- 795 Akaike, H. (1974). A new look at the statistical model identification. *IEEE Transactions on Automatic*
796 *Control*, 19(6), 716–723. <https://doi.org/10.1109/TAC.1974.1100705>
- 797 Almazroui, M., Saeed, F., Saeed, S., Nazrul Islam, M., Ismail, M., Klutse, N. A. B., & Siddiqui, M. H.
798 (2020). Projected Change in Temperature and Precipitation Over Africa from CMIP6. *Earth*
799 *Systems and Environment*, 4(3), 455–475. <https://doi.org/10.1007/s41748-020-00161-x>
- 800 Andersson, J., Pechlivanidis, I., Gustafsson, D., Donnelly, C., & Arheimer, B. (2015). Key factors for
801 improving large-scale hydrological model performance. *European Water*, 49, 77–88.
- 802 Arnell, N. W., & Gosling, S. N. (2016). The impacts of climate change on river flood risk at the global
803 scale. *Climatic Change*, 134(3), 387–401. <https://doi.org/10.1007/s10584-014-1084-5>
- 804 Awotwi, A., Annor, T., Anornu, G. K., Quaye-Ballard, J. A., Agyekum, J., Ampadu, B., Nti, I. K.,
805 Gyampo, M. A., & Boakye, E. (2021). Climate change impact on streamflow in a tropical basin
806 of Ghana, West Africa. *Journal of Hydrology: Regional Studies*, 34, 100805.
807 <https://doi.org/10.1016/j.ejrh.2021.100805>
- 808 Babaousmail, H., Ayugi, B. O., Ojara, M., Ngoma, H., Oduro, C., Mumo, R., & Ongoma, V. (2023).
809 Evaluation of CMIP6 models for simulations of diurnal temperature range over Africa. *Journal*
810 *of African Earth Sciences*, 202, 104944. <https://doi.org/10.1016/j.jafrearsci.2023.104944>
- 811 Berger, V. W., & Zhou, Y. (2014). Kolmogorov–Smirnov Test: Overview. In R. S. Kenett, N. T.
812 Longford, W. W. Piegorsch, & F. Ruggeri (Eds.), *Wiley StatsRef: Statistics Reference Online*
813 (1st ed.). Wiley. <https://doi.org/10.1002/9781118445112.stat06558>
- 814 Biaou, S., Gouwakinnou, G. N., Noulèkoun, F., Salako, K. V., Houndjo Kpoviwanou, J. M. R.,
815 Houehanou, T. D., & Biaou, H. S. S. (2023). Incorporating intraspecific variation into species
816 distribution models improves climate change analyses of a widespread West African tree
817 species (*Pterocarpus erinaceus* Poir, Fabaceae). *Global Ecology and Conservation*, 45, e02538.
818 <https://doi.org/10.1016/j.gecco.2023.e02538>
- 819 Bichet, A., Diedhiou, A., Hingray, B., Evin, G., Touré, N. E., Browne, K. N. A., & Kouadio, K. (2020).
820 Assessing uncertainties in the regional projections of precipitation in CORDEX-AFRICA.
821 *Climatic Change*, 162(2), 583–601. <https://doi.org/10.1007/s10584-020-02833-z>
- 822 Blanchet, J., Molinié, G., & Touati, J. (2018). Spatial analysis of trend in extreme daily rainfall in
823 southern France. *Climate Dynamics*, 51(3), 799–812. <https://doi.org/10.1007/s00382-016-3122-7>
- 824
- 825 Bodian, A., Diop, L., Panthou, G., Dacosta, H., Deme, A., Dezetter, A., Ndiaye, P. M., Diouf, I., &
826 Vischel, T. (2020). Recent Trend in Hydroclimatic Conditions in the Senegal River Basin.
827 *Water*, 12(2), Article 2. <https://doi.org/10.3390/w12020436>
- 828 Brunner, M. I., Slater, L., Tallaksen, L. M., & Clark, M. (2021). Challenges in modeling and predicting
829 floods and droughts: A review. *WIREs Water*, 8(3), e1520. <https://doi.org/10.1002/wat2.1520>
- 830



- 831 Chagnaud, G., Panthou, G., Vischel, T., & Lebel, T. (2023). Capturing and Attributing the Rainfall
832 Regime Intensification in the West African Sahel with CMIP6 Models. *Journal of Climate*,
833 36(6), 1823–1843. <https://doi.org/10.1175/jcli-d-22-0412.1>
- 834 Chagnaud, G., Panthou, G., Vischel, T., & Lebel, T. (2022). A synthetic view of rainfall intensification
835 in the West African Sahel. *Environmental Research Letters*, 17(4), 044005.
836 <https://doi.org/10.1088/1748-9326/ac4a9c>
- 837 Coles, S. (2001). *An introduction to statistical modeling of extreme values*. Springer.
- 838 CRED. (2022). *2021 Disasters in numbers*. Brussels: CRED.
839 https://www.cred.be/sites/default/files/2021_EMDAT_report.pdf
- 840 Davie, J. C. S., Falloon, P. D., Kahana, R., Dankers, R., Betts, R., Portmann, F. T., Wisser, D., Clark,
841 D. B., Ito, A., Masaki, Y., Nishina, K., Fekete, B., Tessler, Z., Wada, Y., Liu, X., Tang, Q.,
842 Hagemann, S., Stacke, T., Pavlick, R., ... Arnell, N. (2013). Comparing projections of future
843 changes in runoff from hydrological and biome models in ISI-MIP. *Earth System Dynamics*,
844 4(2), 359–374. <https://doi.org/10.5194/esd-4-359-2013>
- 845 Dawson, C. W., Abrahart, R. J., Shamseldin, A. Y., Wilby, R. L., & See, L. M. (2005). Neural network
846 modelling of the 20-year flood event for catchments across the UK. *Proceedings. 2005 IEEE*
847 *International Joint Conference on Neural Networks, 2005.*, 4, 2637–2642.
848 <https://doi.org/10.1109/IJCNN.2005.1556319>
- 849 De Longueville, F., Ozer, P., Gemenne, F., Henry, S., Mertz, O., & Nielsen, J. Ø. (2020). Comparing
850 climate change perceptions and meteorological data in rural West Africa to improve the
851 understanding of household decisions to migrate. *Climatic Change*, 160(1), 123–141.
852 <https://doi.org/10.1007/s10584-020-02704-7>
- 853 Diallo, A., Donkor, E., & Owusu, V. (2020). Climate change adaptation strategies, productivity and
854 sustainable food security in southern Mali. *Climatic Change*, 159(3), 309–327.
855 <https://doi.org/10.1007/s10584-020-02684-8>
- 856 Diop S.B., Trambly Y., Bodian A., Ekolu J., Rouché N., Dieppois B., 2025. Flood frequency analysis
857 in West Africa, *Journal of Flood Risk Management*, 18: e70001.
858 <https://doi.org/10.1111/jfr3.70001>
- 859 Dosio, A., Jones, R. G., Jack, C., Lennard, C., Nikulin, G., & Hewitson, B. (2019). What can we know
860 about future precipitation in Africa? Robustness, significance and added value of projections
861 from a large ensemble of regional climate models. *Climate Dynamics*, 53(9), 5833–5858.
862 <https://doi.org/10.1007/s00382-019-04900-3>
- 863 Dosio, A., Jury, M. W., Almazroui, M., Ashfaq, M., Diallo, I., Engelbrecht, F. A., Klutse, N. A. B.,
864 Lennard, C., Pinto, I., Sylla, M. B., & Tamoffo, A. T. (2021). Projected future daily
865 characteristics of African precipitation based on global (CMIP5, CMIP6) and regional
866 (CORDEX, CORDEX-CORE) climate models. *Climate Dynamics*, 57(11), 3135–3158.
867 <https://doi.org/10.1007/s00382-021-05859-w>
- 868 Dotse, S.-Q., Larbi, I., Limantol, A. M., Asare-Nuamah, P., Frimpong, L. K., Alhassan, A.-R. M.,
869 Sarpong, S., Angmor, E., & Ayisi-Addo, A. K. (2023). Rainfall Projections from Coupled
870 Model Intercomparison Project Phase 6 in the Volta River Basin: Implications on Achieving
871 Sustainable Development. *Sustainability*, 15(2), Article 2. <https://doi.org/10.3390/su15021472>
- 872 ECOWREX. (2018). *Ecowas Observatory For Renewable Energy And Energy Efficiency Projects*.
873 Projects <http://www.ecowrex.org/resources/projects>
- 874 Ehret, U., Zehe, E., Wulfmeyer, V., Warrach-Sagi, K., & Liebert, J. (2012). HESS Opinions “Should
875 we apply bias correction to global and regional climate model data?” *Hydrology and Earth*
876 *System Sciences*, 16(9), 3391–3404. <https://doi.org/10.5194/hess-16-3391-2012>
- 877 Ekolu, J., Dieppois, B., Trambly, Y., Villarini, G., Slater, L. J., Mahé, G., Paturel, J.-E., Eden, J. M.,
878 Moulds, S., Sidibe, M., Camberlin, P., Pohl, B., & van de Wiel, M. (2024). Variability in flood



- 879 frequency in sub-Saharan Africa: The role of large-scale climate modes of variability and their
880 future impacts. *Journal of Hydrology*, 640, 131679.
881 <https://doi.org/10.1016/j.jhydrol.2024.131679>
- 882 El Adlouni, S., Ouarda, T. B. M. J., Zhang, X., Roy, R., & Bobée, B. (2007). Generalized maximum
883 likelihood estimators for the nonstationary generalized extreme value model. *Water Resources*
884 *Research*, 43(3). <https://doi.org/10.1029/2005WR004545>
- 885 Elagib, N. A., Zayed, I. S. A., Saad, S. A. G., Mahmood, M. I., Basheer, M., & Fink, A. H. (2021).
886 Debilitating floods in the Sahel are becoming frequent. *Journal of Hydrology*, 599, 126362.
887 <https://doi.org/10.1016/j.jhydrol.2021.126362>
- 888 EM-DAT. (2015). *The OFDA/CRED International Disaster Database. Centre for Research on the*
889 *Epidemiology of Disasters (CRED)*. Université catholique de Louvain. <http://www.emdat.be>
- 890 Engmann, S., & Cousineau, D. (2011). Comparing distributions: The two-sample Anderson–Darling
891 test as an alternative to the Kolmogorov–Smirnov test. *Journal of Applied Quantitative*
892 *Methods*, 6, 1–17.
- 893 Famien, A. M., Janicot, S., Ochou, A. D., Vrac, M., Defrance, D., Sultan, B., & Noël, T. (2018). A bias-
894 corrected CMIP5 dataset for Africa using the CDF-t method – a contribution to agricultural
895 impact studies. *Earth System Dynamics*, 9(1), 313–338. [https://doi.org/10.5194/esd-9-313-](https://doi.org/10.5194/esd-9-313-2018)
896 2018
- 897 Feaster, T. D., Gotvald, A. J., Musser, J. W., Weaver, J. C., Kolb, K., Veilleux, A. G., & Wagner, D.
898 M. (2023). Magnitude and frequency of floods for rural streams in Georgia, South Carolina,
899 and North Carolina, 2017—Results. In *Scientific Investigations Report (2023–5006)*. U.S.
900 Geological Survey. <https://doi.org/10.3133/sir20235006>
- 901 Fisher, R. A. (1992). Statistical Methods for Research Workers. In S. Kotz & N. L. Johnson (Eds.),
902 *Breakthroughs in Statistics: Methodology and Distribution* (pp. 66–70). Springer.
903 https://doi.org/10.1007/978-1-4612-4380-9_6
- 904 Flaounas, E., Drobinski, P., Vrac, M., Bastin, S., Lebeaupin-Brossier, C., Stéfanon, M., Borga, M., &
905 Calvet, J.-C. (2013). Precipitation and temperature space–time variability and extremes in the
906 Mediterranean region: Evaluation of dynamical and statistical downscaling methods. *Climate*
907 *Dynamics*, 40(11), 2687–2705. <https://doi.org/10.1007/s00382-012-1558-y>
- 908 Frieler, K., Lange, S., Piontek, F., Reyer, C. P. O., Schewe, J., Warszawski, L., Zhao, F., Chini, L.,
909 Denvil, S., Emanuel, K., Geiger, T., Halladay, K., Hurtt, G., Mengel, M., Murakami, D.,
910 Ostberg, S., Popp, A., Riva, R., Stevanovic, M., ... Yamagata, Y. (2017). Assessing the impacts
911 of 1.5 °C global warming – simulation protocol of the Inter-Sectoral Impact Model
912 Intercomparison Project (ISIMIP2b). *Geoscientific Model Development*, 10(12), 4321–4345.
913 <https://doi.org/10.5194/gmd-10-4321-2017>
- 914 Gudmundsson, L., Wagener, T., Tallaksen, L. M., & Engeland, K. (2012). Evaluation of nine large-
915 scale hydrological models with respect to the seasonal runoff climatology in Europe. *Water*
916 *Resources Research*, 48(11). <https://doi.org/10.1029/2011WR010911>
- 917 Gumbel, E. J. (1958). *Statistics of Extremes*. Columbia University Press.
918 <https://doi.org/10.7312/gumb92958>
- 919 Hamdi, Y., Duluc, C.-M., & Rebour, V. (2018). Temperature Extremes: Estimation of Non-Stationary
920 Return Levels and Associated Uncertainties. *Atmosphere*, 9(4), Article 4.
921 <https://doi.org/10.3390/atmos9040129>
- 922 Hamed, K. H., & Rao, A. R. (1998). A modified Mann-Kendall trend test for autocorrelated data.
923 *Journal of Hydrology*, 204, 182–196. [https://doi.org/10.1016/S0022-1694\(97\)00125-X](https://doi.org/10.1016/S0022-1694(97)00125-X)
- 924 Han, X., Mehrotra, R., Sharma, A., & Rahman, A. (2022). Incorporating nonstationarity in regional
925 flood frequency analysis procedures to account for climate change impact. *Journal of*
926 *Hydrology*, 612, 128235. <https://doi.org/10.1016/j.jhydrol.2022.128235>



- 927 Hansen, J., Ruedy, R., Sato, M., & Lo, K. (2010). GLOBAL SURFACE TEMPERATURE CHANGE.
928 *Reviews of Geophysics*, 48(4). <https://doi.org/10.1029/2010RG000345>
- 929 Hawkins, E., & Sutton, R. (2009). The Potential to Narrow Uncertainty in Regional Climate Predictions.
930 *Bulletin of the American Meteorological Society*, 90(8), 1095–1108.
931 <https://doi.org/10.1175/2009BAMS2607.1>
- 932 Hawkins, E., & Sutton, R. (2012). Time of emergence of climate signals. *Geophysical Research Letters*,
933 39(1). <https://doi.org/10.1029/2011GL050087>
- 934 Heinicke, S., Volkholz, J., Schewe, J., Gosling, S. N., Schmied, H. M., Zimmermann, S., Mengel, M.,
935 Sauer, I. J., Burek, P., Chang, J., Kou-Giesbrecht, S., Grillakis, M., Guillaumot, L., Hanasaki,
936 N., Koutroulis, A., Otta, K., Qi, W., Satoh, Y., Stacke, T., ... Frieler, K. (2024). Global
937 hydrological models continue to overestimate river discharge. *Environmental Research Letters*,
938 19(7), 074005. <https://doi.org/10.1088/1748-9326/ad52b0>
- 939 Hochberg, Y., & Benjamini, Y. (1995). Controlling the false discovery rate: A practical and powerful
940 approach to multiple testing. *JR Stat Soc*, 57(1), 289–300.
- 941 Hosking, J. R. M. (1990). L-Moments: Analysis and Estimation of Distributions Using Linear
942 Combinations of Order Statistics. *Journal of the Royal Statistical Society: Series B*
943 *(Methodological)*, 52(1), 105–124. <https://doi.org/10.1111/j.2517-6161.1990.tb01775.x>
- 944 Hossain, A., Mathias, C., & Blanton, R. (2021). Remote Sensing of Turbidity in the Tennessee River
945 Using Landsat 8 Satellite. *Remote Sensing*, 2021, 3785. <https://doi.org/10.3390/rs13183785>
- 946 Houghton, J. E. T., Ding, Y., Griggs, D., Noguier, M., van der Linden, P., Dai, X., Maskell, M., &
947 Johnson, C. (2001). Climate Change 2001: The Scientific Basis. In *Contribution of Working*
948 *Group I to the Third Assessment Report of the Intergovernmental Panel on Climate Change*
949 *(IPCC): Vol. 881*. (p. 881).
- 950 Huang, X., Yin, J., Slater, L. J., Kang, S., He, S., & Liu, P. (2024). Global Projection of Flood Risk
951 With a Bivariate Framework Under 1.5–3.0°C Warming Levels. *Earth's Future*, 12(4),
952 e2023EF004312. <https://doi.org/10.1029/2023EF004312>
- 953 IPCC. (2021). *Sixth Assessment Report (AR6): Climate Change 2021: The Physical Science Basis*.
954 Cambridge University Press.
- 955 Jayaweera, L., Wasko, C., & Nathan, R. (2024). Modelling non-stationarity in extreme rainfall using
956 large-scale climate drivers. *Journal of Hydrology*, 636, 131309.
957 <https://doi.org/10.1016/j.jhydrol.2024.131309>
- 958 Katz, R. W. (2013). Statistical Methods for Nonstationary Extremes. In A. AghaKouchak, D. Easterling,
959 K. Hsu, S. Schubert, & S. Sorooshian (Eds.), *Extremes in a Changing Climate: Detection,*
960 *Analysis and Uncertainty* (pp. 15–37). Springer Netherlands. [https://doi.org/10.1007/978-94-](https://doi.org/10.1007/978-94-007-4479-0_2)
961 [007-4479-0_2](https://doi.org/10.1007/978-94-007-4479-0_2)
- 962 Kauffeldt, A., Halldin, S., Rodhe, A., Xu, C.-Y., & Westerberg, I. K. (2013). Disinformative data in
963 large-scale hydrological modelling. *Hydrology and Earth System Sciences*, 17(7), 2845–2857.
964 <https://doi.org/10.5194/hess-17-2845-2013>
- 965 Kendall, M. G. (1975). *Rank correlation methods* (4th ed., 2d impression). Griffin London.
- 966 Khaliq, M. N., Ouarda, T. B. M. J., Gachon, P., Sushama, L., & St-Hilaire, A. (2009). Identification of
967 hydrological trends in the presence of serial and cross correlations: A review of selected
968 methods and their application to annual flow regimes of Canadian rivers. *Journal of Hydrology*,
969 368(1), 117–130. <https://doi.org/10.1016/j.jhydrol.2009.01.035>
- 970 Klutse, N. A. B., Quagraine, K. A., Nkrumah, F., Quagraine, K. T., Berkoh-Oforiwa, R., Dzrobi, J. F.,
971 & Sylla, M. B. (2021). The Climatic Analysis of Summer Monsoon Extreme Precipitation
972 Events over West Africa in CMIP6 Simulations. *Earth Systems and Environment*, 5(1), 25–41.
973 <https://doi.org/10.1007/s41748-021-00203-y>
- 974 Krishnamurthy, P. K., Lewis, K., & Choularton, R. K. (2012). *Climate impacts on food security and*



- 975 *nutrition—A review of existing knowledge*. Met Office and WFP’s Office for Climate Change,
976 Environment and Disaster Risk Reduction: Exeter, UK.
- 977 Lalou, R., Sultan, B., Muller, B., & Ndonky, A. (2019). Does climate opportunity facilitate smallholder
978 farmers’ adaptive capacity in the Sahel? *Palgrave Communications*, 5(1), 1–11.
979 <https://doi.org/10.1057/s41599-019-0288-8>
- 980 Land, V. van der, Romankiewicz, C., & Geest, K. van der. (2018). Environmental change and migration:
981 A review of West African case studies. In *Routledge Handbook of Environmental Displacement*
982 *and Migration*. Routledge.
- 983 Lange, S. (2018). Bias correction of surface downwelling longwave and shortwave radiation for the
984 EWEMBI dataset. *Earth System Dynamics*, 9(2), 627–645. [https://doi.org/10.5194/esd-9-627-](https://doi.org/10.5194/esd-9-627-2018)
985 2018
- 986 Lange, S. (2019). *Earth2Observe, WFDEI and ERA-Interim data Merged and Bias-corrected for*
987 *ISIMIP (EWEMBI)* (Version 1.1, p. 1 Files) [Application/octet-stream]. GFZ Data Services.
988 <https://doi.org/10.5880/PIK.2019.004>
- 989 Lawrence, D. (2020). Uncertainty introduced by flood frequency analysis in projections for changes in
990 flood magnitudes under a future climate in Norway. *Journal of Hydrology: Regional Studies*,
991 28, 100675. <https://doi.org/10.1016/j.ejrh.2020.100675>
- 992 Lee, H., Calvin, K., Dasgupta, D., Krinner, G., Mukherji, A., Thorne, P., Trisos, C., Romero, J.,
993 Aldunce, P., Barret, K., & others. (2023). *IPCC, 2023: Climate Change 2023: Synthesis Report,*
994 *Summary for Policymakers. Contribution of Working Groups I, II and III to the Sixth*
995 *Assessment Report of the Intergovernmental Panel on Climate Change [Core Writing Team,*
996 *H. Lee and J. Romero (eds.)]. IPCC, Geneva, Switzerland.*
- 997 Mann, H. B. (1945). Nonparametric Tests Against Trend. *Econometrica*, 13(3), 245.
998 <https://doi.org/10.2307/1907187>
- 999 Martins, E. S., & Stedinger, J. R. (2000). Generalized maximum-likelihood generalized extreme-value
1000 quantile estimators for hydrologic data. *Water Resources Research*, 36(3), 737–744.
1001 <https://doi.org/10.1029/1999WR900330>
- 1002 Masson-Delmotte, V. P., Zhai, P., Pirani, S. L., Connors, C., Péan, S., Berger, N., Caud, Y., Chen, L.,
1003 Goldfarb, M. I., & Scheel Monteiro, P. M. (2021). *IPCC, 2021: Summary for Policymakers.*
1004 *In: Climate Change 2021: The Physical Science Basis. Contribution of Working Group I to the*
1005 *Sixth Assessment Report of the Intergovernmental Panel on Climate Change [Report].*
1006 Cambridge University Press, Cambridge, United Kingdom and New York, NY, USA.
1007 <https://researchspace.csir.co.za/dspace/handle/10204/12710>
- 1008 Matthew, O. A., Owolabi, O. A., Osabohien, R., Urhie, E., Ogunbiyi, T., Olawande, T. I., Edafe, O. D.,
1009 & Daramola, P. J. (2020). Carbon Emissions, Agricultural Output and Life Expectancy in West
1010 Africa. *International Journal of Energy Economics and Policy*, 10(3), Article 3.
- 1011 Michelangeli, P.-A., Vrac, M., & Loukos, H. (2009). Probabilistic downscaling approaches:
1012 Application to wind cumulative distribution functions. *Geophysical Research Letters*, 36(11).
1013 <https://doi.org/10.1029/2009GL038401>
- 1014 Monerie, P.-A., Dittus, A. J., Wilcox, L. J., & Turner, A. G. (2023). Uncertainty in Simulating
1015 Twentieth Century West African Precipitation Trends: The Role of Anthropogenic Aerosol
1016 Emissions. *Earth’s Future*, 11(2), e2022EF002995. <https://doi.org/10.1029/2022EF002995>
- 1017 Mudge, J. F., Baker, L. F., Edge, C. B., & Houlihan, J. E. (2012). Setting an Optimal α That Minimizes
1018 Errors in Null Hypothesis Significance Tests. *PLOS ONE*, 7(2), e32734.
1019 <https://doi.org/10.1371/journal.pone.0032734>
- 1020 Muñoz-Sabater, J., Dutra, E., Agustí-Panareda, A., Albergel, C., Arduini, G., Balsamo, G., Boussetta,
1021 S., Choulga, M., Harrigan, S., Hersbach, H., Martens, B., Miralles, D. G., Piles, M., Rodríguez-
1022 Fernández, N. J., Zsoter, E., Buontempo, C., & Thépaut, J.-N. (2021). ERA5-Land: A state-of-



- 1023 the-art global reanalysis dataset for land applications. *Earth System Science Data*, 13(9), 4349–
1024 4383. <https://doi.org/10.5194/essd-13-4349-2021>
- 1025 Nicholson, S. E. (2018). Climate of the Sahel and West Africa. In S. E. Nicholson, *Oxford Research*
1026 *Encyclopedia of Climate Science*. Oxford University Press.
1027 <https://doi.org/10.1093/acrefore/9780190228620.013.510>
- 1028 Nka, B. N., Oudin, L., Karambiri, H., Paturel, J. E., & Ribstein, P. (2015). Trends in floods in West
1029 Africa: Analysis based on 11 catchments in the region. *Hydrology and Earth System Sciences*,
1030 19(11), 4707–4719. <https://doi.org/10.5194/hess-19-4707-2015>
- 1031 Noël, T., Loukos, H., Defrance, D., Vrac, M., & Levvasseur, G. (2022). Extending the global high-
1032 resolution downscaled projections dataset to include CMIP6 projections at increased resolution
1033 coherent with the ERA5-Land reanalysis. *Data in Brief*, 45, 108669.
1034 <https://doi.org/10.1016/j.dib.2022.108669>
- 1035 Nooni, I. K., Ogou, F. K., Chaibou, A. A. S., Nakoty, F. M., Gnitou, G. T., & Lu, J. (2023). Evaluating
1036 CMIP6 Historical Mean Precipitation over Africa and the Arabian Peninsula against Satellite-
1037 Based Observation. *Atmosphere*, 14(3), Article 3. <https://doi.org/10.3390/atmos14030607>
- 1038 O’Neill, B. C., Krieglner, E., Ebi, K. L., Kemp-Benedict, E., Riahi, K., Rothman, D. S., van Ruijven, B.
1039 J., van Vuuren, D. P., Birkmann, J., Kok, K., Levy, M., & Solecki, W. (2017). The roads ahead:
1040 Narratives for shared socioeconomic pathways describing world futures in the 21st century.
1041 *Global Environmental Change*, 42, 169–180. <https://doi.org/10.1016/j.gloenvcha.2015.01.004>
- 1042 Orange, D. (1990). *Hydroclimatologie du Fouta Djallon et dynamique actuelle d’un vieux paysage*
1043 *latéritique (Afrique de l’Ouest)*.
- 1044 Panthou, G., Vischel, T., Lebel, T., Quantin, G., Pugin, A.-C. F., Blanchet, J., & Ali, A. (2013). From
1045 pointwise testing to a regional vision: An integrated statistical approach to detect
1046 nonstationarity in extreme daily rainfall. Application to the Sahelian region. *Journal of*
1047 *Geophysical Research: Atmospheres*, 118(15), 8222–8237. <https://doi.org/10.1002/jgrd.50340>
- 1048 Papalexioiu, S. M., & Koutsoyiannis, D. (2013). Battle of extreme value distributions: A global survey
1049 on extreme daily rainfall. *Water Resources Research*, 49(1), 187–201.
1050 <https://doi.org/10.1029/2012WR012557>
- 1051 Pechlivanidis, I. G., Arheimer, B., Donnelly, C., Hundedcha, Y., Huang, S., Aich, V., Samaniego, L.,
1052 Eisner, S., & Shi, P. (2017). Analysis of hydrological extremes at different hydro-climatic
1053 regimes under present and future conditions. *Climatic Change*, 141(3), 467–481.
1054 <https://doi.org/10.1007/s10584-016-1723-0>
- 1055 Pierce, D. W., Cayan, D. R., Maurer, E. P., Abatzoglou, J. T., & Hegewisch, K. C. (2015). Improved
1056 Bias Correction Techniques for Hydrological Simulations of Climate Change. *Journal of*
1057 *Hydrometeorology*, 16(6), 2421–2442. <https://doi.org/10.1175/JHM-D-14-0236.1>
- 1058 Pospichal, B., Karam, D. B., Crewell, S., Flamant, C., Hünerbein, A., Bock, O., & Saïd, F. (2010).
1059 Diurnal cycle of the intertropical discontinuity over West Africa analysed by remote sensing
1060 and mesoscale modelling. *Quarterly Journal of the Royal Meteorological Society*, 136(S1), 92.
1061 <https://doi.org/10.1002/qj.435>
- 1062 Prosdocimi, I., & Kjeldsen, T. (2021). Parametrisation of change-permitting extreme value models and
1063 its impact on the description of change. *Stochastic Environmental Research and Risk*
1064 *Assessment*, 35(2), 307–324. <https://doi.org/10.1007/s00477-020-01940-8>
- 1065 Prudhomme, C., Zsótér, E., Matthews, G., Melet, A., Grimaldi, S., Zuo, H., Hansford, E., Harrigan, S.,
1066 Mazzetti, C., de Boisseson, E., Salamon, P., & Garric, G. (2024). Global hydrological
1067 reanalyses: The value of river discharge information for world-wide downstream applications
1068 – The example of the Global Flood Awareness System GloFAS. *Meteorological Applications*,
1069 31(2), e2192. <https://doi.org/10.1002/met.2192>
- 1070 Rai, S., Hoffman, A., Lahiri, S., Nychka, D. W., Sain, S. R., & Bandyopadhyay, S. (2024). Fast



- 1071 parameter estimation of generalized extreme value distribution using neural networks.
1072 *Environmetrics*, 35(3), e2845. <https://doi.org/10.1002/env.2845>
- 1073 Rameshwaran, P., Bell, V. A., Brown, M. J., Davies, H. N., Kay, A. L., Rudd, A. C., & Sefton, C.
1074 (2022). Use of Abstraction and Discharge Data to Improve the Performance of a National-Scale
1075 Hydrological Model. *Water Resources Research*, 58(1), e2021WR029787.
1076 <https://doi.org/10.1029/2021WR029787>
- 1077 Rameshwaran, P., Bell, V. A., Davies, H. N., & Kay, A. L. (2021). How might climate change affect
1078 river flows across West Africa? *Climatic Change*, 169(3), 21. [https://doi.org/10.1007/s10584-](https://doi.org/10.1007/s10584-021-03256-0)
1079 [021-03256-0](https://doi.org/10.1007/s10584-021-03256-0)
- 1080 Riahi, K., van Vuuren, D. P., Kriegler, E., Edmonds, J., O'Neill, B. C., Fujimori, S., Bauer, N., Calvin,
1081 K., Dellink, R., Fricko, O., Lutz, W., Popp, A., Cuaresma, J. C., Kc, S., Leimbach, M., Jiang,
1082 L., Kram, T., Rao, S., Emmerling, J., ... Tavoni, M. (2017). The Shared Socioeconomic
1083 Pathways and their energy, land use, and greenhouse gas emissions implications: An overview.
1084 *Global Environmental Change*, 42, 153–168. <https://doi.org/10.1016/j.gloenvcha.2016.05.009>
- 1085 Rodríguez-Fonseca, B., Mohino, E., Mechoso, C. R., Caminade, C., Biasutti, M., Gaetani, M., Garcia-
1086 Serrano, J., Vizy, E. K., Cook, K., Xue, Y., Polo, I., Losada, T., Druyan, L., Fontaine, B., Bader,
1087 J., Doblas-Reyes, F. J., Goddard, L., Janicot, S., Arribas, A., ... Voldoire, A. (2015). Variability
1088 and Predictability of West African Droughts: A Review on the Role of Sea Surface Temperature
1089 Anomalies. *Journal of Climate*, 28(10), 4034–4060. [https://doi.org/10.1175/JCLI-D-14-](https://doi.org/10.1175/JCLI-D-14-00130.1)
1090 [00130.1](https://doi.org/10.1175/JCLI-D-14-00130.1)
- 1091 Roudier, P., Sultan, B., Quirion, P., & Berg, A. (2011). The impact of future climate change on West
1092 African crop yields: What does the recent literature say? *Global Environmental Change*, 21(3),
1093 1073–1083. <https://doi.org/10.1016/j.gloenvcha.2011.04.007>
- 1094 Santer, B. D., Bonfils, C. J. W., Fu, Q., Fyfe, J. C., Hegerl, G. C., Mears, C., Painter, J. F., Po-Chedley,
1095 S., Wentz, F. J., Zelinka, M. D., & Zou, C.-Z. (2019). Celebrating the anniversary of three key
1096 events in climate change science. *Nature Climate Change*, 9(3), 180–182.
1097 <https://doi.org/10.1038/s41558-019-0424-x>
- 1098 Sauer, I. J., Reese, R., Otto, C., Geiger, T., Willner, S. N., Guillod, B. P., Bresch, D. N., & Frieler, K.
1099 (2021). Climate signals in river flood damages emerge under sound regional disaggregation.
1100 *Nature Communications*, 12(1), 2128. <https://doi.org/10.1038/s41467-021-22153-9>
- 1101 Scholz, F. W., & Stephens, M. A. (1986). K-Sample Anderson-Darling Tests of Fit, for Continuous and
1102 Discrete Cases, Technical Report. *University of Washington, Seattle*.
- 1103 Sillmann, J., Kharin, V. V., Zhang, X., Zwiers, F. W., & Bronaugh, D. (2013). Climate extremes indices
1104 in the CMIP5 multimodel ensemble: Part 1. Model evaluation in the present climate. *Journal*
1105 *of Geophysical Research: Atmospheres*, 118(4), 1716–1733.
1106 <https://doi.org/10.1002/jgrd.50203>
- 1107 Song, J.-H., Her, Y., & Kang, M.-S. (2022). Estimating Reservoir Inflow and Outflow From Water
1108 Level Observations Using Expert Knowledge: Dealing With an Ill-Posed Water Balance
1109 Equation in Reservoir Management. *Water Resources Research*, 58(4), e2020WR028183.
1110 <https://doi.org/10.1029/2020WR028183>
- 1111 Srivast, A. K., Rahimi, J., Alsafadi, K., Vianna, M., Enders, A., Zheng, W., Demircan, A., Dieng, M.
1112 D. B., Salack, S., Faye, B., Singh, M., Ewert, F., & Gaiser, T. (2023). *Dynamic Modelling of*
1113 *Mixed Crop-Livestock Systems: A Case Study of Climate Change Impacts in sub-Saharan*
1114 *Africa*. <https://doi.org/10.21203/rs.3.rs-3793846/v1>
- 1115 Stedinger, J. R., & Griffis, V. W. (2011). Getting From Here to Where? Flood Frequency Analysis and
1116 Climate. *JAWRA Journal of the American Water Resources Association*, 47(3), 506–513.
1117 <https://doi.org/10.1111/j.1752-1688.2011.00545.x>
- 1118 Sule, I. M., & Odekunle, M. O. (2016). *Landscapes of West Africa: A Window on a Changing World*.



- 1119 CILLS: Landscapes of West Africa: A Window on a Changing World. US
- 1120 Sultan, B., & Gaetani, M. (2016). Agriculture in West Africa in the Twenty-First Century: Climate
1121 Change and Impacts Scenarios, and Potential for Adaptation. *Frontiers in Plant Science*, 7.
1122 <https://doi.org/10.3389/fpls.2016.01262>
- 1123 Tarpanelli, A., Paris, A., Sichangi, A. W., O'Loughlin, F., & Papa, F. (2023). Water Resources in
1124 Africa: The Role of Earth Observation Data and Hydrodynamic Modeling to Derive River
1125 Discharge. *Surveys in Geophysics*, 44(1), 97–122. [https://doi.org/10.1007/s10712-022-09744-](https://doi.org/10.1007/s10712-022-09744-x)
1126 x
- 1127 Tian, C., Huang, G., Lu, C., Song, T., Wu, Y., & Duan, R. (2023). Northward Shifts of the Sahara
1128 Desert in Response to Twenty-First-Century Climate Change. *Journal of Climate*, 36(10),
1129 3417–3435. <https://doi.org/10.1175/JCLI-D-22-0169.1>
- 1130 Totin, E., Padgham, J., Ayivor, J., Dietrich, K., Fosu-Mensah, B., Gordon, C., Habtezion, S.,
1131 Tweneboah Lawson, E., Mensah, A., Nukpezah, D., Ofori, B., Piltz, S., Sidibé, A., Sissoko,
1132 M., Traore, P., Dazé, A., & Echeverría, D. (2016). *Vulnerability and Adaptation to Climate*
1133 *Change in Semi-Arid Areas in West Africa*. <https://doi.org/10.13140/RG.2.2.15263.87202>
- 1134 Taylor, C. M., Belušić, D., Guichard, F., Parker, D. J., Vischel, T., Bock, O., Harris, P. P., Janicot, S.,
1135 Klein, C., & Panthou, G. (2017). Frequency of extreme Sahelian storms tripled since 1982 in
1136 satellite observations. *Nature*, 544 (7651), 475–478. <https://doi.org/10.1038/nature22069>
- 1137 Trambly Y., Villarini G., Wei Z., 2020. Observed changes in flood hazard in Africa. *Environmental*
1138 *Research Letters*, 15, 1040b5, <https://doi.org/10.1088/1748-9326/abb90b>
- 1139 Trambly, Y., El Khalki, E. M., Khedimallah, A., Sadaoui, M., Benaabidate, L., Boulmaiz, T.,
1140 Boutaghane, H., Dakhlaoui, H., Hanich, L., Ludwig, W., Meddi, M., Elmehdi Saidi, M., &
1141 Mahé, G. (2024). Regional flood frequency analysis in North Africa. *Journal of Hydrology*,
1142 630, 130678. <https://doi.org/10.1016/j.jhydrol.2024.130678>
- 1143 Trambly, Y., Rouché, N., Paturel, J.-E., Mahé, G., Boyer, J.-F., Amoussou, E., Bodian, A., Dacosta,
1144 H., Dakhlaoui, H., Dezetter, A., Hughes, D., Hanich, L., Peugeot, C., Tshimanga, R., &
1145 Lachassagne, P. (2021). ADHI: The African Database of Hydrometric Indices (1950–2018).
1146 *Earth System Science Data*, 13(4), 1547–1560. <https://doi.org/10.5194/essd-13-1547-2021>
- 1147 Trambly, Y., & Somot, S. (2018). Future evolution of extreme precipitation in the Mediterranean.
1148 *Climatic Change*, 151(2), 289–302. <https://doi.org/10.1007/s10584-018-2300-5>
- 1149 UNDRR. (2023). *Annual Report 2023*. United Nations Office for Disaster Risk Reduction.
- 1150 UNEP. (2020). *Water Scarcity in Sub-Saharan Africa*. United Nations Environment Programme.
- 1151 Van Der Knijff, J. M., Younis, J., & De Roo, A. P. J. (2010). LISFLOOD: A GIS-based distributed
1152 model for river basin scale water balance and flood simulation. *International Journal of*
1153 *Geographical Information Science*, 24(2), 189–212.
1154 <https://doi.org/10.1080/13658810802549154>
- 1155 Vintrou, E. (2012). *Cartographie et caractérisation des systèmes agricoles au Mali par télédétection à*
1156 *moyenne résolution spatiale* [PhD Thesis]. AgroParisTech.
- 1157 Wasko, C., Westra, S., Nathan, R., Orr, H. G., Villarini, G., Villalobos Herrera, R., & Fowler, H. J.
1158 (2021). Incorporating climate change in flood estimation guidance. *Philosophical Transactions*
1159 *of the Royal Society A: Mathematical, Physical and Engineering Sciences*, 379(2195),
1160 20190548. <https://doi.org/10.1098/rsta.2019.0548>
- 1161 Wilcox, C., Vischel, T., Panthou, G., Bodian, A., Blanchet, J., Descroix, L., Quantin, G., Cassé, C.,
1162 Tanimoun, B., & Kone, S. (2018). Trends in hydrological extremes in the Senegal and Niger
1163 Rivers. *Journal of Hydrology*, 566, 531–545. <https://doi.org/10.1016/j.jhydrol.2018.07.063>
- 1164 Wilks, D. S. (2006). On “Field Significance” and the False Discovery Rate. *Journal of Applied*
1165 *Meteorology and Climatology*, 45(9), 1181–1189. <https://doi.org/10.1175/JAM2404.1>
- 1166 Wilks, D. S. (2016). “The Stippling Shows Statistically Significant Grid Points”: How Research Results



- 1167 are Routinely Overstated and Overinterpreted, and What to Do about It. *Bulletin of the*
1168 *American Meteorological Society*, 97(12), 2263–2273. <https://doi.org/10.1175/BAMS-D-15->
1169 00267.1
- 1170 World Bank. (2021a). *An EPIC response: Innovative governance for Flood and Drought Risk*
1171 *Management*. World Bank.
- 1172 World Bank. (2021b). World Bank Engagement in Transboundary Waters in West Africa:
1173 Retrospective and Lessons Learned. *World Bank, Washington, DC*.